EVALUATING THE FEASIBILITY AND EFFECTIVENESS OF A MEASUREMENT DEVICE TO BE USED INTRAOPERATIVELY DURING AORTIC VALVE REPAIR

ROHAIL QURESHI

Thesis submitted to the University of Ottawa
in partial Fulfillment of the requirements for the
Master of Applied Science (MASc) in Biomedical Engineering

Department of Mechanical Engineering
Faculty of Engineering
University of Ottawa

ABSTRACT

The ability to accurately and in a repeatable fashion, measure aortic valve dimensions during aortic valve repair is critical to the restoration of function in a diseased aortic valve, as for example in aortic insufficiency. Although several methods for measuring aortic valve dimensions have been shown to be feasible, they are approximate and lack the accuracy, robustness, and repeatability one would expect to support aortic valve repair surgery. In addition, they do not allow for the intra-operative measurement of aortic valves under conditions equivalent to the physiological (pressurized) state. A prototype medical device was designed, and 3-D printed at the University of Ottawa that would allow cardiac surgeons performing aortic valve repair to do just that. The prototype was tested for its accuracy and precision at the University of Ottawa Heart Institute using porcine aortic valves. Based on unsatisfactory results of this experimentation, namely, that the device was applying forces that were too large, a numerical simulation study was designed using a commercial finite element software LS-DYNA. This simulation study was used to explore the forces that the prototype device needed to apply to obtain end-diastolic pressurized dimensions of the aortic valve. The simulation study showed that one single device was likely not possible to obtain measurements in an aortic valve. However, a system of two devices could be imagined, one to measure the STJ diameter and free margin length of the aortic valve cusps, and one to measure the cusp height of the same valve, for the purposes of aortic valve repair.

TABLE OF CONTENTS

LIST OF FIGURES

LIST OF TABLES

1 INTRODUCTION

The aortic valve (AV) is normally made of three rather symmetrical cusps that open during contraction of the heart (systole) for blood evacuation, and close during relaxation of the heart (diastole). The AV cusps are attached inside the proximal part of the ascending aorta (the aortic root) which balloons out around each of the cusps' attachments, creating the three aortic sinuses. Aortic insufficiency is a condition of the heart that is characterized by the incomplete closure of the AV. This results in some of the blood ejected by the left ventricle into the aorta during systole, to leak back into the ventricle during diastole. This leakage prevents the efficient pumping of oxygenated blood to the body, and may cause symptoms such as fatigue, shortness of breath and angina [1]. One approach to treating aortic insufficiency is AV repair which leaves as much as possible of the original tissue intact and aims to correct the dimensions of the AV components to ensure proper AV functioning after surgery.

1.1 RATIONALE FOR RESEARCH

Surgeons operate on unpressurized valves during open-heart surgery and need to guess the large dimensional changes in the AV when under physiological pressures, which is very challenging. As computer simulations are becoming available to provide dimensional guidelines for reconstruction of the AV [2,3], there is a critical need for the intraoperative measurement of the AV components, such that surgeons can effectively implement the guidelines.

1.2 OBJECTIVES

The objectives of this study were to first test a new prototype for the intraoperative measurement of AV components, and then based on the results, provide leads to potentially enhance, modify, and redesign the device.

1.3 CONTRIBUTIONS

The existing prototype, although available, had not yet been tested for its effectiveness in terms of accuracy and precision for determining AV dimensions. Both accuracy and precision needed to be evaluated to determine the tool's efficacy and reliability for AV repair procedures.

With the help of an echocardiographer and two cardiology residents, the prototype was tested on porcine AVs at the University of Ottawa Heart Institute (UOHI). To determine "ground-truth" dimensions of the normal pig valves, all the valves were artificially statically pressurized to 80 mmHg and their cusp dimensions were obtained using 3D echocardiography (TEE), which is recognized by clinicians as providing measurements with good accuracy and precision. Then, to determine the effectiveness of the tool, various dimensions were measured both by different participants and in a repeated fashion, using the prototype. This allowed for post-experimental analysis of both the accuracy and precision of the device. It was determined that the prototype was in fact not producing AV dimensions that were consistent with the "ground-truth" dimensions obtained from TEE. More specifically, the dimensions obtained by the device were considerably larger than those obtained from imaging.

Following this conclusion, a study based on numerical simulations in normal and diseased human AVs was designed to determine specific forces (as would be applied by the tool) that could approximate in-vivo loads in the AV to reproduce in-vivo dimensions. Using a set of previously collected 3D-TEE images of human AVs and their corresponding unpressurized 3D finite element models, arbitrary forces at specific points were introduced. Many simulations were run until post-process analysis yielded satisfactory agreement between the in-vivo dimensions of the AV components determined from 3D-TEE imaging and those resulting from the forces applied in the finite element models of the unpressurized valves. In total, simulations were run on 12 valves and analysis of the results provided a better understanding of what well chosen point loads could replicate in-vivo dimensions in the unpressurized AV.

From the analysis of the simulation results, it was demonstrated that a system of two devices could be imagined, that when used together, would allow for the accurate measurement of the AV

components' critical dimensions, namely the sinotubular junction diameter, and the free margin length and height of each individual cusp.

1.4 THESIS ORGANIZATION

This document reports on the motivation, background, methods, analysis, results, and conclusions of the research performed regarding the application, effectiveness, and methods for improving a prototype AV measurement device especially useful for treating aortic insuffiency.

There are six main chapters to this report: the introduction, the literature review, a description of the experimental testing of the prototype measurement device, an overview of the computer simulation study, a discussion of the results, and conclusions. The introduction sets the foundation for the forthcoming material and provides the reader with the motivation and objectives of the research. The literature review introduces some anatomy, physiology, and pathology of the AV as well as the concepts underlying AV repair. Further, it outlines the power of computer simulations for AV repair as well as current methods for AV repair but also identifies the current knowledge gap in the field. The next two chapters outline the exploratory phase of the research: first, an experiment with the prototype device to gain a better understanding of its effectiveness and second, a computer simulation study to better understand the required loading on AVs to achieve end-diastolic dimensions and determine whether this loading is in fact compatible with how the prototype measurement device has been designed to function. The next two sections discuss the implications of the research performed, and what can consequently be said of the current prototype and any future work in this area. The conclusion will highlight how this research may benefit AV repair and what is potentially left to be explored.

2 LITERATURE REVIEW

It is important to review several topics to familiarize the reader with the background anatomy and physiology related to the project. As such, the anatomy and physiology of the AV will be explained in this chapter as well as some pathologies of the AV and surgical techniques to treat them. Furthermore, the concept of AV repair will be discussed in detail as well as the use of computer simulations in the context of AV repair surgery, and finally, measurement methods currently used during AV repair.

Lastly, this chapter will provide details on what significant work has already been done in this area and what is missing. This knowledge gap will ultimately be the motivation for the present research, as will be illustrated in later chapters.

2.1 ANATOMY AND PHYSIOLOGY OF THE AV

A central component of the human cardiovascular system is the heart. The heart acts like a pump, which forces blood to flow through the arterial system under pressure [4]. To accomplish this task, the heart is made up of four chambers, two atria and two ventricles (Figure 1). The left and right atria receive blood from the venous circulation and the left and right ventricles eject blood into the arterial system [4]. When the blood returns to the heart via the pulmonary veins, it passes through the left atrium and then the left ventricle [4]. From the left ventricle, it is ejected into the aorta for circulation through the systemic arteries to the rest of the body [4].

The circulation of blood throughout the heart and the cardiovascular system is achieved by the cardiac cycle, a pattern of rhythmic movements the heart undergoes that alternately contract, forcing blood out of its chambers and relax, allowing its chambers to refill with blood [4]. Systole refers to the period of contraction while diastole refers to the period of relaxation. The cardiac cycle is marked by a series of pressure and blood volume changes in the chambers of the heart [4]. When pressure in the heart is low, blood returning from circulation flows passively into the atria through the open atrioventricular valves while the aortic and pulmonary valves (Figure 1) remain closed [4]. Once enough blood is filled into the ventricles, the atria relax, and the atrioventricular

valves begin to close [4]. The ventricles then begin contracting while the ventricular pressure rises rapidly and when this pressure exceeds the pressure of the downstream arteries, the semilunar valves (aortic and pulmonary valves) are forced open and blood rushes into the aorta and pulmonary trunk [4]. It is important to note that the heart's two sets of valves are unidirectional, preventing the backward flow of blood. These valves are supported by connective fibrous tissue [4]. Both the atrioventricular and semilunar valves open and close depending on the pressure differences on either side of the valves [4]. The aortic semilunar valve was the focus of this study.

The AV is located between the left ventricle and the aorta [4]. It acts as a gateway for oxygenated blood to travel to the rest of the body's organs. The AV opens during left ventricular contraction (systole) to allow blood flow into the aorta and closes during ventricular relaxation (diastole) to prevent backwards flow of blood [4]. Figures 3 and 4 show three-dimensional schematic representations of the AV. The AV consists of the aortic root which is the structure characterized by the transition between the left ventricular outflow tract and the ascending aorta [4]. The aortic root is mainly composed of the three sinuses of Valsalva, which are located between the ventriculoaortic junction (VAJ) and the sinotubular junction (STJ) (Figure 4). The sinuses of Valsava are outwardly ballooned regions of the aortic wall (Figure 3) [4]. In each of the three sinuses, there is a leaflet, or cusp [4]. Normally, an AV consists of three cusps (Figures 3 and 4), the right coronary cusp, the left coronary cusp and the noncoronary cusp [4]. The base of each cusp is attached to the aortic root but is also fused with the adjacent cusps on both lateral sides. [4]. The commissures are the regions where two cusps insert side by side along parallel lines (Figures 3 and 4).

As the AV closes at the end of systole, the cusps collapse against each other (Figure 3) [5] until they make enough contact to find an equilibrium configuration against the difference in blood pressure between the aorta and the left ventricle [4]. The contact surface area is called the coaptation surface and in healthy closed AVs, the cusps coapt in a well aligned manner (at the centre of the orifice) (Figure 3) [5], thus preventing backflow of blood into the left ventricle [4]. The typical variation in blood pressure in the AV ranges from 80 mmHg in diastole to 120 mmHg in systole.

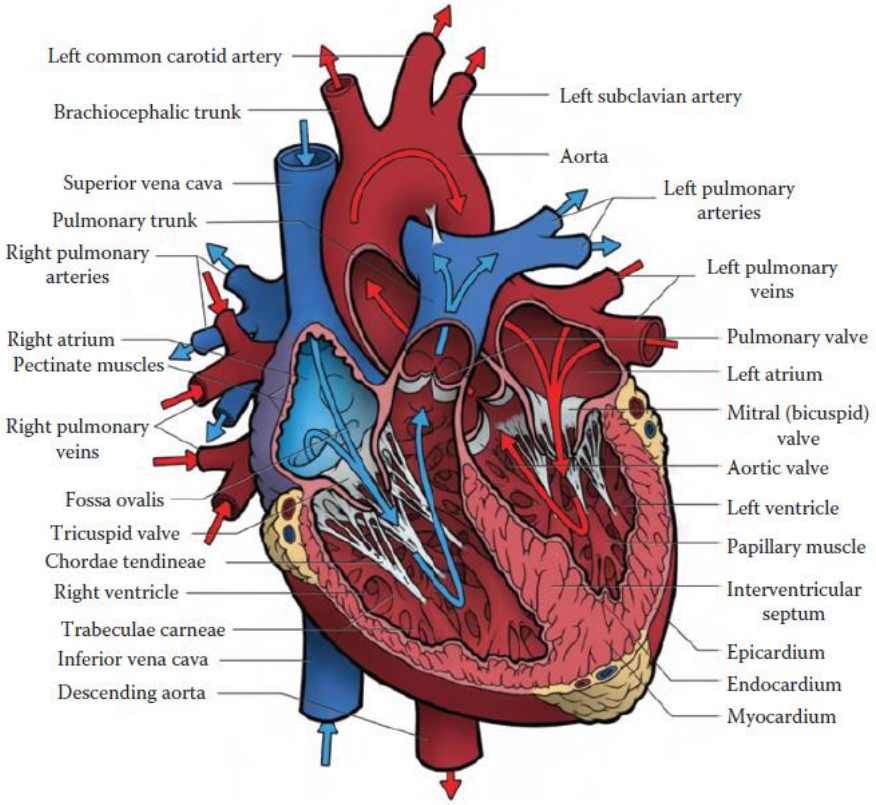

Figure 1: The human heart [5].

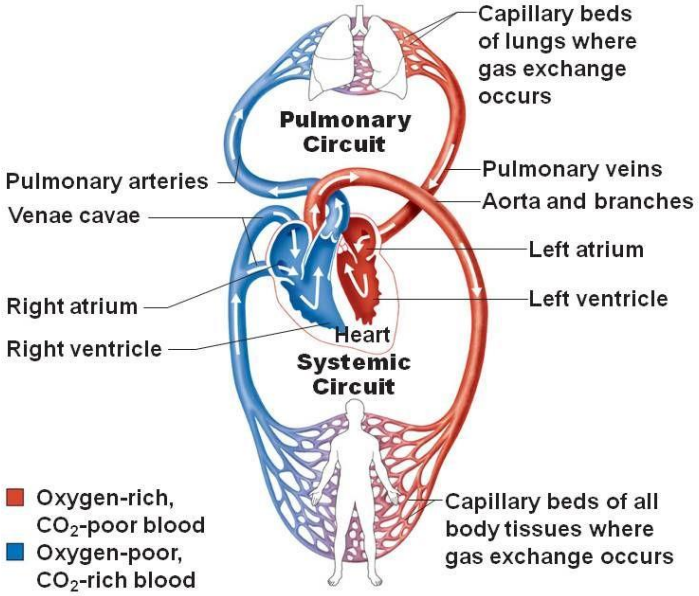

Figure 2: The pulmonary circuit and the systemic circuit [4].

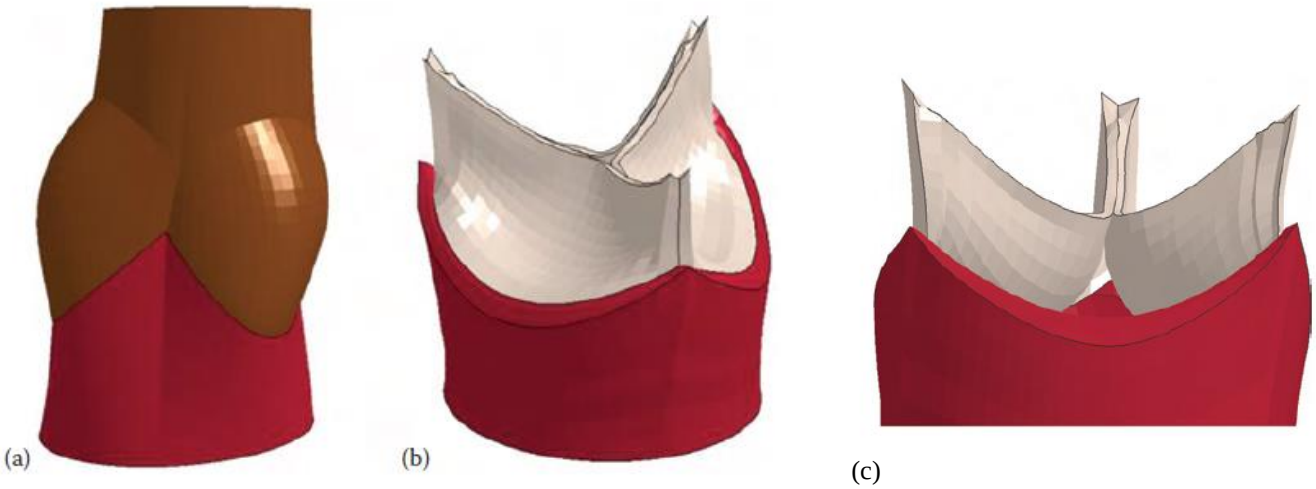

Figure 3: The AV: (a) Full view, with the sinuses of Valsalva and proximal ascending aorta shown in brown, and an idealized ventriculoaortic junction shown in red; (b) Perspective view of the AV cusps in closed position; (c) Side view, with one cusp removed [5]

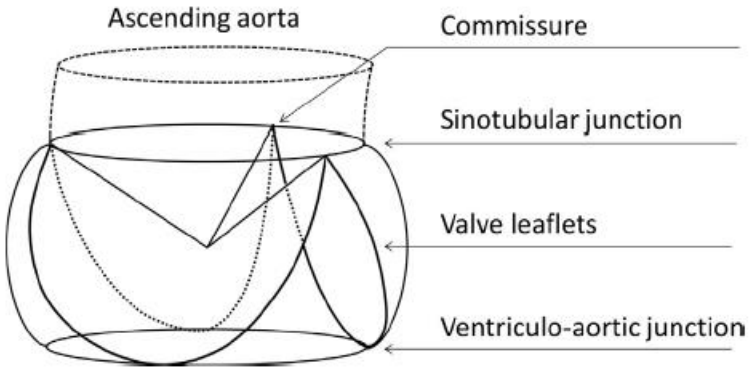

Figure 4: The AV skeleton view [6]

2.2 PATHOLOGY AND SURGERY OF THE AV

There are relatively common diseases that can manifest in the AV, namely aortic stenosis and aortic insuffiency [5]. Aortic stenosis (AS) occurs when the AV opening during systole is narrowed [5]. This ultimately produces a less than ideal outflow of the left ventricle [5]. The cause of AS can be a congenital abnormality of the valve or progressive calcification [5]. Due to the elevated

pressures in the left ventricle during systole, and the attempt to maintain the same cardiac output despite the stenotic outflow tract, the left ventricle undergoes a hypertrophic process (the muscular wall thickens) [5]. Apart from congenital abnormality, AS is uncommon in the population aged under 65 years [7]. However, in the United States, the prevalence is about 5% in the population at 65 years old and increases with age [7]. A meta-analysis, conducted in the United States, Europe and Taiwan showed a population prevalence of AS of 12.4% [7]. The treatment for AS tends to be AV replacement with a mechanical or bioprosthetic valve through open-heart surgery [7], or trans-catheter implantation of a bioprosthetic valve (TAVI), when the patient cannot be safely operated on by open-heart surgery [5]. The procedure for AV replacement is systematic and no complex and detailed dimensions for example, need to be measured before, during, or after the surgery. On the other hand, where AV repair is possible in the case of another AV disease called aortic insufficiency, which is described next, these parameters may need to be accounted for.

Aortic regurgitation, also known as aortic insuffiency (AI), is a type of AV disease characterized by the incomplete closure of the valve in diastole [5]. This results in blood flowing in the reverse direction (or leaking) back into the left ventricle after the completion of systole during the cardiac cycle. AI can be caused by several factors, including but not limited to, aortic dilatation, congenital abnormality of the valve and calcification [5]. The return of blood from the aorta into the left ventricle increases the ventricular workload through pressure and volume overloads, which in turn trigger a hypertrophic dilatation of the left ventricle [5]. This leakage therefore prevents the efficient pumping of oxygenated blood to the body, and may present symptoms in the patient as fatigue, shortness of breath and angina [1].

Classifications of AI failure mechanisms are generally based on the distinction between two causes for AI, namely, problems with the aortic root and issues with the cusps [5]. Both these mechanisms affect the coaptation performance (how well the AV completely closes) and generate a regurgitant orifice and a regurgitant “jet” through that orifice (Figure 5) [5]. The first category is based on the normal motion of the cusps [5]. Most of these cases involve dilatation of specific locations of the aortic root, enlargement of the sinotubular junction diameter (STJ), dilatation of the sinuses of Valsalva and the STJ, or dilatation of the ventriculoaortic junction (VAJ). Furthermore, cusp perforation can also be classified into this first category [5]. Dilatation affecting the aortic root will inevitably increase the distance between the commissures and may result in incomplete, or

incompetent AV closure. The second and third categories are determined based on the major cusp-failure mechanisms [5]. The second category describes cusp prolapse, which is defined as the displacement of the free edge (also called free margin) of a cusp down to below the coaptation area of other normal cusps (Figure 6) [5]. The last category designates cusp restriction, where cusp mobility is reduced because of malformation, calcification, thickening, or fibrosis of the cusp [5].

These failure mechanisms illustrate the level and depth of understanding of the malfunctioning of the valve, as required by a surgeon wishing to repair an AV. However, to be able to return the diseased valve to a correct structure and, therefore, function, very precise dimensions in the AV must be measured. This is to be able to accurately capture the geometric descriptions of the malformed valves before, after, and possibly during the surgery, in each unique patient. As a result, successful treatment, and repair of the AV in AI cases characterized by the failure mechanisms described above, should ideally be done with the help of some sort of instrument, such as the prototype measurement device envisioned in this work.

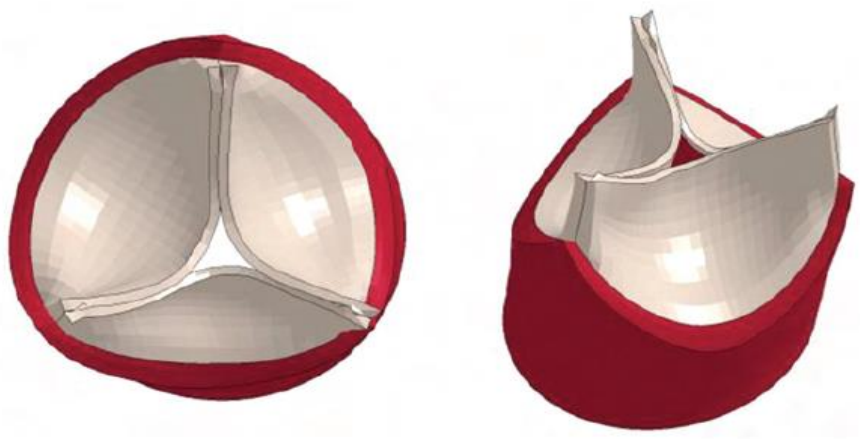

Figure 5: Depiction of regurgitant orifice and non-ideal coaptation in aortic cusps]5].

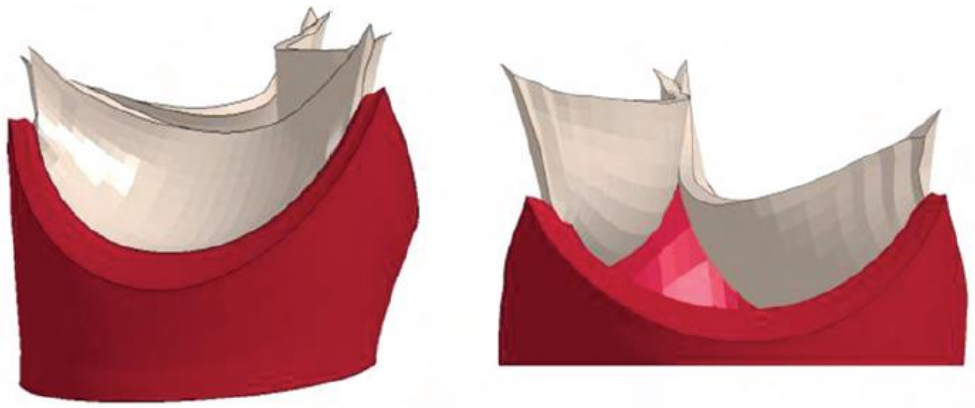

Figure 6: Depiction of aortic cusp prolapse. On the right, one cusp was removed for a better appreciation of the prolapse]5].

2.3 AV REPAIR

There are two main surgical methods used for the treatment of AV disease [5]. The first method is the replacement of the original AV by a prosthetic valve, either a mechanical or a bioprosthetic valve [5]. Mechanical valves are prone to damaging red blood cells and inducing blood clotting due to their rigid structure, and as a result, patients who receive such valves need to be treated with life-long anticoagulation therapy [5]. On the other hand, bioprosthetic valves are derived from porcine or bovine AVs and have their living cells destroyed to avoid host rejection by the patient's immune system [5]. The consequence of the absence of living cells in bioprosthetic valves is that they are unable to self-repair as normal living tissues do, and as such, the useful life of these valves is only around 10-15 years [5].

While AS typically damages the valve beyond repair and justifies surgical AV replacement or a TAVI procedure, AI normally does not exhibit a major structural degradation of the tissues. In fact, for AI, valve repair is now seen as a viable alternative to complete replacement because both methods show similar durability and safety [5]. In addition, valve repair avoids or minimizes the risks associated with prosthetic valve replacement, including long-term anticoagulation related hemorrhage, structural deterioration, clot formation, and valve infection late after surgery [5]. The

main goal of AV repair is to restore normal functional configuration to the native diseased valve [5].

AV repair can be generally divided into two categories, aortic root procedures and cusp corrections [5]. The objective of the former category is the correction of various type of aortic root dilatations that render the AV dysfunctional [5]. In addition to, or in lieu of aortic root procedures, the aortic cusps may need to be corrected due to abnormal geometry and therefore function [5]. There are different repair techniques that can be used to address the above problems. Aortic root procedures have the common goal of preserving the patients' AV cusps while repairing the aortic root components [5]. The most common aortic root procedures are the David procedure and the Yacoub procedure [5]. Both procedures involve graft tubing to replace the biological tissues of the original aortic root [5]. In both cases the aortic root is removed and replaced by sewing along the cusps' attachment lines [5]. The David procedure (reimplantation) involves suturing the graft along the VAJ and resuspending the original commissures inside the tube graft (Figure 7a) [5]. The Yacoub procedure (remodeling) on the other hand, involves suturing a tailored graft tube along the residual sewing margin (Figure 7b) [5]. Finally, when dilatation of the VAJ after the surgery is of concern, a sub commissural annuloplasty, as seen in Figure 7c can be performed to maintain appropriate dimensions of the VAJ [5].

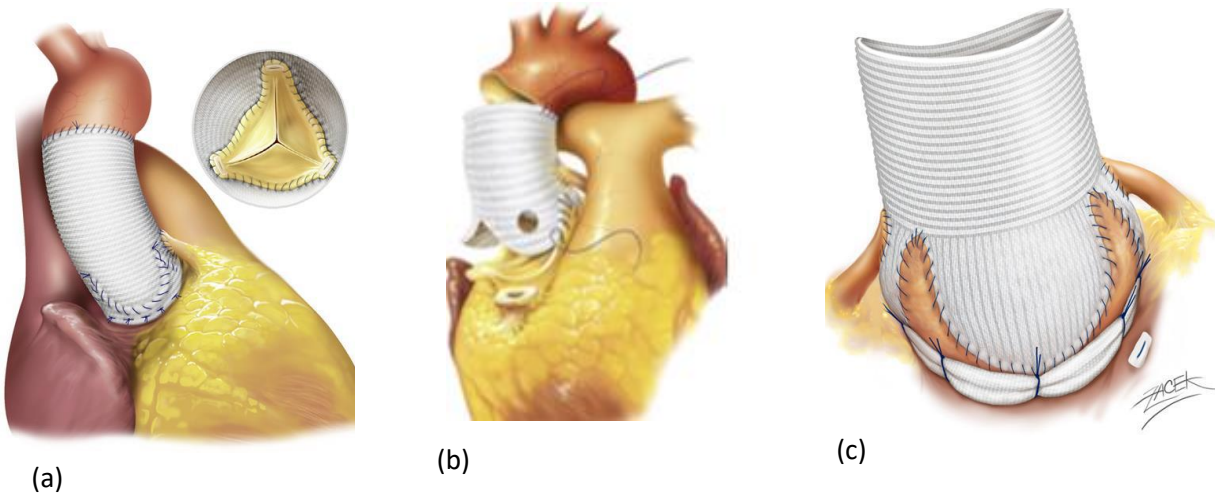

Figure 7: AV Repair Techniques, (a) Reimplantation (b) Remodeling (c) Remodeling + Annuloplasty]8]

When cusp corrections are needed, the main goal is to correct the cusp prolapsing, since this is the most frequent cusp pathology [5]. Two common surgical techniques that are employed are cusp resuspension and plication, which both aim to reduce the length of the cusp free margin length [5]. The former procedure involves a continuous suture along the length of the free-margin and then applying traction to the suture to reduce and stabilize the free margin (Figure 8) [5]. On the other hand, plication aims to reduce the excess free margin along the cusp by "folding it on the aortic side by tying a "suture" (Figure 8) [5]. The plication technique can be central (folded along the middle of the free margin) or commissural (folded along the commissures of the valve) [5].

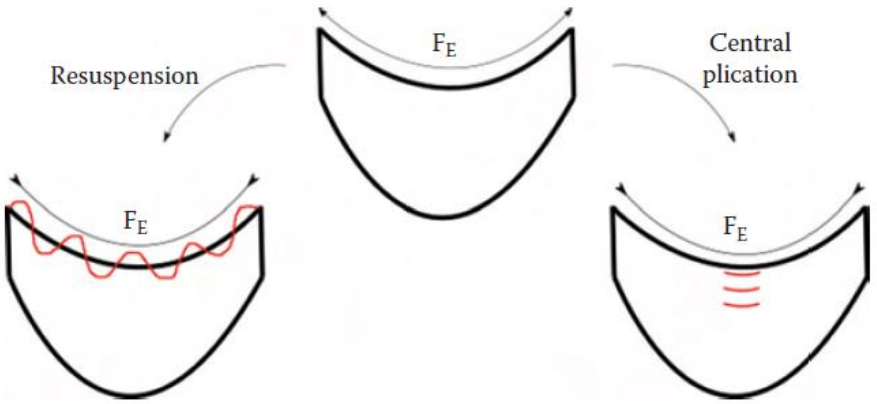

Figure 8: AV cusp correction techniques: cusp free-margin resuspension (left) and central plication (right). FE: cusp free margin]5].

Regardless of the approach, in any of the methods used for AV repair discussed above, the knowledge of the geometry of the native diseased valve is crucial [5]. This is because the geometry of the AV is very important to its function [5]. Thus, for the successful repair of the AV to its functional configuration, it is necessary to know and to be able to accurately measure the dimensions of the valve. As shown in Figure 9, these dimensions include, but are not limited to, the free margin length of the cusps (the curvilinear distance that runs on top of each cusp connecting the two commissures common to that cusp), the valve height (the straight-line distance between the VAJ and the STJ planes), the straight-line distance between the commissures, the cusp height (the curvilinear distance from the attachment point of each cusp to the middle of the free margin of that cusp (G_H in Figure 9), and the sinotubular junction (STJ) diameter (see Figure 9) [5].

Although some dimensional information about the valves can be available preoperatively through imaging, it is ultimately in the operating room, during surgery, that the surgeon can measure all the valve components with best accuracy to ensure correct restoration [9]. However, measuring the cusps proves to be difficult due to the ease with which they stretch and deform. Nonetheless, many solutions have been proposed to allow aortic cusp measurement in the operating room to enhance the chances for perfect restoration of valve competence post-surgery [9]. However, even with these tools, the AV dimensions to correct diseases such as AI cannot be measured accurately nor in a repeatable fashion. These measurement tools and methods will be discussed in Section 2.5 below.

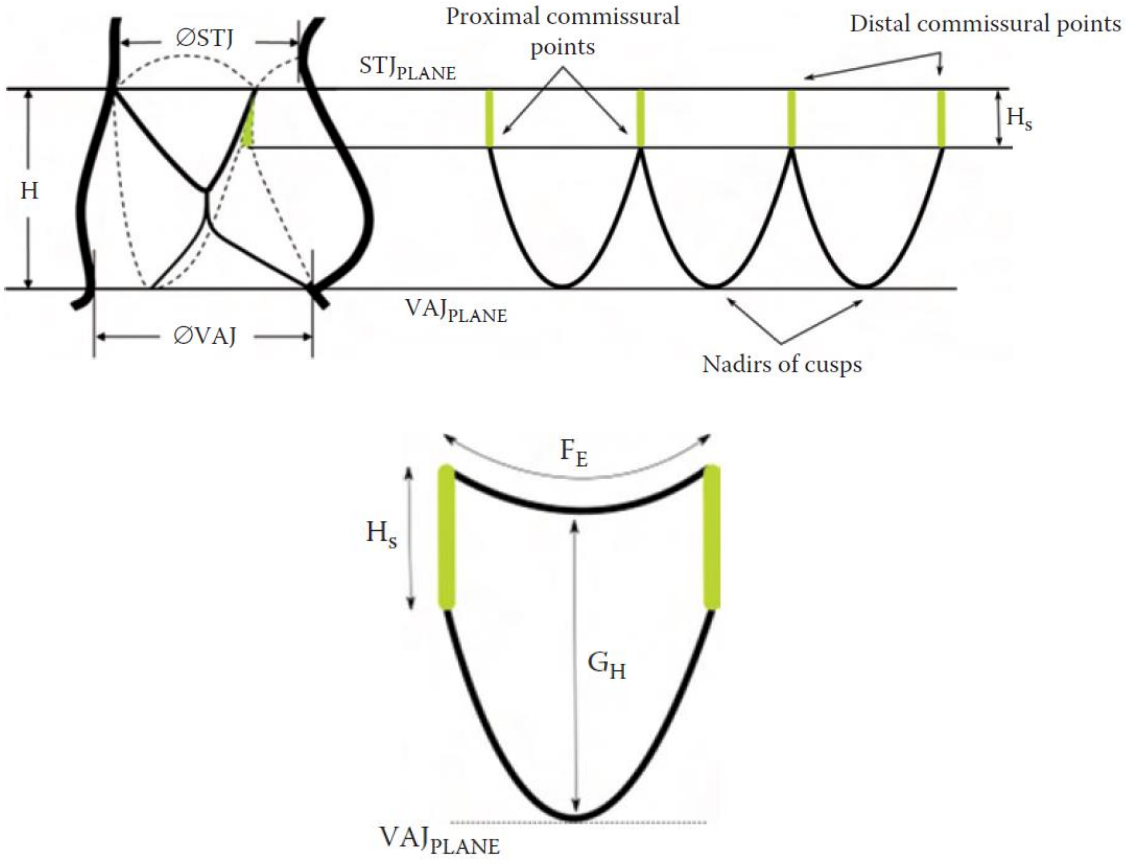

Figure 9: Depiction of AV showing detailed geometry: STJ and VAJ diameters as well as valve height (H) are depicted (top) and Valve cusp showing notably the cusp free margin length (F_E) and the cusp height (G_H) (bottom)]5].

2.4 COMPUTER SIMULATION FOR AV REPAIR

Although indications for AV repair are rising, many AI cases still undergo replacement because of the lack of surgical expertise and training available for AV repair [10]. The main reasons why this is the case include the incomplete understanding of the pathoanatomy and pathophysiology of AI, and the inability to use preoperative findings for intraoperative assessment [10]. Furthermore, it is the "lack of predictability in the outcome of the surgical techniques employed, and the irreproducibility of results of AV repair by different surgeons" [10]. The valve is repaired unpressurized and during this process shows vastly different dimensions than those under physiological pressure. Therefore, after surgical repair, the valve may still not function correctly. Because of this uncertainty, it is difficult for surgeons to accurately predict the outcome of AV repair [10]. Surgeons therefore need a method of predictive simulation of the repaired AV to "ascertain its overall function" after the valve repair operation [10].

In the clinical imaging world, transesophageal echocardiography (TEE) has been shown to be superior to the traditional magnetic resonance imaging (MRI) or computed tomography (CT) studies done to provide high resolution 4-D scans of the AV over the cardiac cycle [10]. Further, "lately, finite element (FE) models have been used to explore AV mechanics, and compare the reimplantation and remodelling techniques" [10]. However, many of the studies do not account for the fact that AV repair is done on an unpressurized valve [10]. A 2015 study titled *Subject-specific finite-element modeling of normal AV biomechanics from 3D+t TEE images* by Labrosse et al. looked to determine the "feasibility of assessing the AV biomechanics in a subject-specific manner" [10]. In this study, as a first step, the researchers demonstrated valve mechanics on normal intact valves and addressed the complexities involved with AV geometry, the impracticability of determining the material properties of the AV material and the necessity to determine unpressurized geometry for finite element modelling [10]. Essentially, the process involved extracting geometrical information about the AV from "four dimensional" images namely, the three-dimensional shape of the valve changing through time (3D+t TEE), then building a finite-element (FE) model of the AV [10]. Further, material properties were estimated for the aorta and the AV leaflets according to the age of the patient, and this information was used to find suitable unpressurized dimensions for the AV [10]. Finally, "intra-and inter-operator variability in manual measurements was assessed and the proposed methodology tested and discussed" [10].

The first step in this study was to determine the AV configuration from 3D+t TEE images. These images allowed for the estimation of the AV anatomy in late diastole thanks to the time ("t") aspect of the imaging. The AV model that was constructed using this technique consisted of the outflow tract of the left ventricle, the AV cusps, the sinuses of Valsalva, and the proximal ascending aorta [10]. There were 21 landmarks that were extracted from the images using a graphical user interface named AVQ which was designed in MATLAB (Figure 10) [10]. After selecting key landmarks from the imaging as prompted to by the program, 3D surfaces and volumes are constructed from the selected landmarks using finite element method algorithms [10]. After selecting further landmarks and key times during the cardiac cycle, the information is processed, and important structural dimensions of the AV are determined [10]. This information is then used to build a finite-element discretization (mesh) leading to a FE model as can be seen in Figure 11 [10].

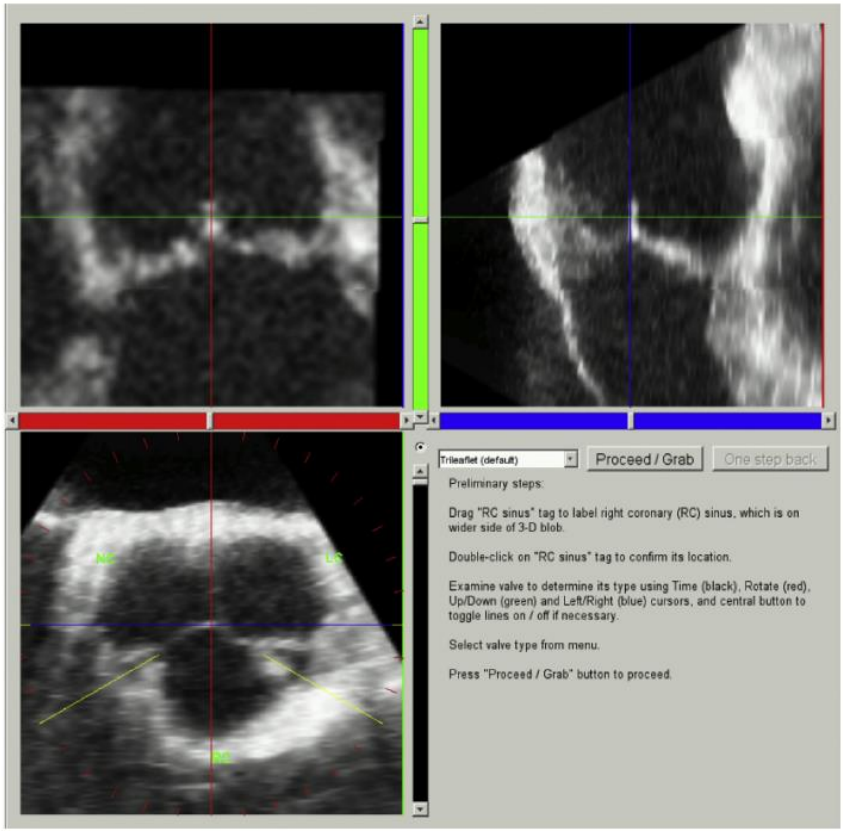

Figure 10: The AVQ program provides step-by-step guidance to the user to look through the AV and select anatomical landmarks [10].

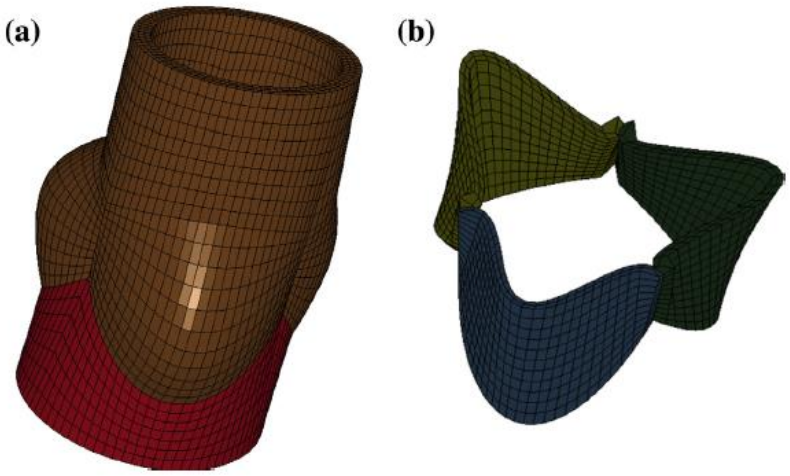

Figure 11: (a) Unpressurized aortic root finite element model; (b) View of the cusps in open position inside the model [10].

Due to limited data available on aortic sinus tissues, "the material properties of the ascending aorta were assumed identical to those of the aortic sinuses" [10]. To determine the material properties of the aortic sinuses in the finite element model, experimental values of circumferential and longitudinal stretch ratios in 14 excised pressurized human ascending aortas under appropriate boundary conditions were used [10]. This was to determine the average circumferential and longitudinal stretch ratios for pressures between 0 and 160 mmHg in two average groups (one at age 54 and one at age 72) [10]. Further, "based on evidence of linear variation of these stretches with age", the circumferential and longitudinal stretch ratios at any given age based on those at 54 and 72 were determined [10]. These data were then used with the fact that the average unpressurized human ascending aortic wall thickness is 1.86 mm, as well as the known patient-specific ascending aortic diameter (through imaging) to calculate the "parameters of a hyperelastic, transversely isotropic material representing the age-matched human ascending aorta" [10]. Namely, the material model was Guccione et al.'s [10].

With regards to the AV cusps, planar equiaxial data published in [11] from porcine AVs (age 6-9 months) and human AVs (average age of 80.6 years) were used [10]. Strains were measured under controlled membrane tensions and averaged for the three aortic leaflets [10]. Furthermore, as suggested in [11], it was assumed that the porcine data was valid to describe aortic leaflets in 18-year-old humans [10]. Similarly, to the aortic sinuses, a linear variation was assumed but this time of the circumferential and radial stretch ratios with age [10]. Furthermore, "the thickness of the

aortic leaflets was linearly interpolated from the human aortic leaflet thickness at age 15 and 85 [10]. This information allowed the researchers to determine the age-matched material constants for the aortic leaflets of the subject using Guccione et al.'s material model, as also mentioned above [10].

This study provides an approach to tackling the problem of subject-specific modeling of normal AV biomechanics [10]. It in fact showed that using the created AVQ program, subject-specific geometry of the AV could be obtained quickly [10]. Furthermore, and thereafter, the AVSim program easily uses the AVQ measurements to create a finite element model of the AV [10]. Finally, using age-matched material properties of the aorta and the aortic leaflets, AVSim iteratively determines the unpressurized geometry modifying the corresponding AV dimensions and running analyses of the AV's dynamic mechanical behaviour during a cardiac cycle [10] until the dimensions of the valve in late diastole match those measured by the AVQ program [10].

All in all, this research was the first mechanism to be able to process subject-specific 3D+t TEE AV data, determine age-matched material properties for the aortic and leaflet tissues and finally, construct a finite element model of an unpressurized AV, and simulate the AV function throughout a cardiac cycle [10]. In particular, the cusp coaptation area, which describes how well the valve seals, correlated well with both the measured valve through imaging and the simulations [10].

Since this publication, the AVSim program has then been supplemented by a module to modify the unpressurized geometry of the valve using different techniques of AV repair, thereby allowing virtual surgery to be done on an originally diseased valve. While this simulation work allows one to produce potentially valuable scenarios for cardiac surgeons to follow, an important issue remains to be solved: the need for the surgeon to be able to accurately implement the dimensions recommended by the simulation.

2.5 MEASUREMENT METHODS IN THE AV

In-vivo measurements of the AV can be taken relatively easily using 3D imaging; however, it seems to be underused. In fact, Siemens has technology available (eSie Valves^{TM}) [12] which allows for cardiologists to measure many valvular dimensions during the cardiac cycle; however, it cannot be used during open-heart valve repair surgery when the heart is depressurized [12].

Although some dimensional information about the valves is available preoperatively, it is ultimately in the operating room, during surgery, that the surgeon can measure all the valve components with best accuracy [5]. Although measuring the cusps proves difficult due to the easiness with which they stretch and deform, several solutions have been proposed to allow cusp measurement in the operating room to enhance the chances for perfect restoration of valve competence [5].

Some dimensions of the valve can already be measured intraoperatively, including the valve diameter (e.g., using a Hegaar sizer) and the so-called effective height of the cusps (e.g., using Schäfers' caliper [13]). However, these, and other partial measurements [14,15], can only be made in the unpressurized valve. The geometric height of the cusps can also be measured by manually applying traction on the cusps; however, how much traction should be applied is unknown, resulting in widely varying dimensions depending on the sources [16]. Similarly, the free margin of the cusps may be measured, e.g., using a thread that is approximated to each free margin before measurement [17]. The process is time-consuming and again, unreliable, because unpressurized cusps are very soft and elastic. During AV repair, cardiac surgeons must visually approximate almost all the corrections needed in the dimensions of the valve components such that they work well together again after surgery [18]. The main goal of AV repair is to make the AV functional again, and all dimensions and their interactions between each other have a significant influence on the AV function [18]. Thus, it is especially important for an effective measurement device to ensure equivalent pressurized dimensions of the AV's components before measuring them. A prototype handheld measurement device was recently designed and 3D-printed at the University of Ottawa (Figure 12). It uses calibrated force application to approximate the pressurized dimensions of the AV, while the valve is unpressurized overall.

The calibrated force application is a key design feature that allows for the "control" of the applied force. The relation in space of the force applicators (as shown with arrows in Figure 12), with the rest of the prototype, was carefully designed using idealized beam bending/deflection properties.

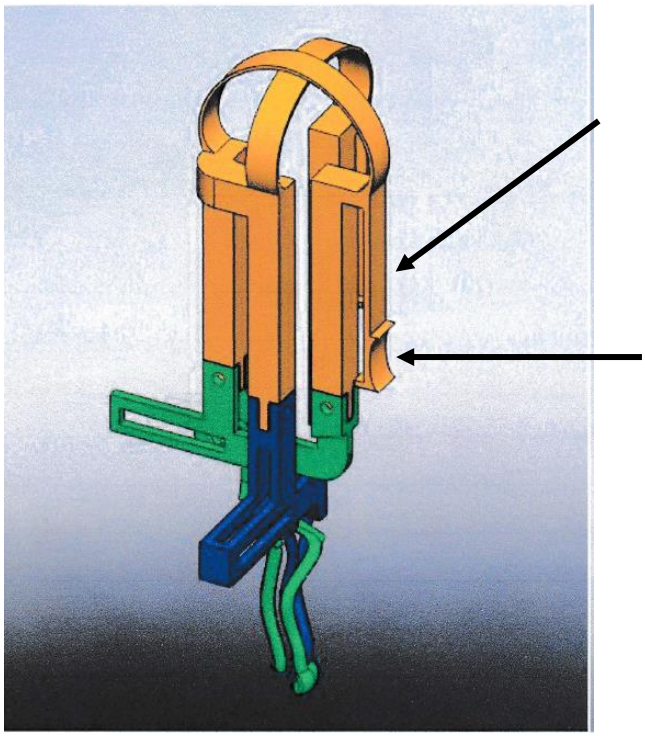

Figure 12: Prototype handheld AV measurement device. Arrows point to force applicators (one can be seen, and one hidden at 90 degrees counter-clockwise) [18]

The valve on which surgeons operate is unpressurized (valve repair is an open-heart procedure) and presents with dimensions that are very different from those under physiological pressure. Therefore, surgeons need to guess the dimensional changes that occur in the valve between the time when they do the surgery, and the time when pressure is re-applied. In the absence of effective, calibrated measuring tools, surgeons have a hard time predicting the outcome of the surgery, cannot guarantee the repeatability of the surgical procedure, and cannot implement dimensional guidelines from simulations that might be available to them. Furthermore, any improvement toward standardization calls for a way to measure the pressurized dimensions of the valve's components. Finally, due to the highly nonlinear behaviour of these tissues, a simple way to predict pressurized dimensions based on unpressurized ones has proven elusive [18].

The measurements directly or indirectly allowed by the invention include the distances between commissures of the valve, the sinotubular junction diameter, as well as the geometric height and free margin length of the cusps [18]. The objective of the device is to obtain measurements in the

operating room in a few minutes, in a repeatable manner [18], to allow the surgeon to measure the original diseased valve, as well as the valve after repair, before blood flow is restored in the patient's heart [18].

This invention is unique also because it is the only known device that allows for the intra-operative measurement of AVs under conditions equivalent to the physiological (pressurized) state [18]. Further, as mentioned above, it provides a comprehensive list of dimensional parameters for the valve components.

Lastly, it is worth mentioning that there exists a study [6] that aimed to determine forces in the aortic root using a force transducer, but the methodology was unfortunately flawed. This was because the researchers had an incorrect assumption regarding the output of the implanted force traducer in the aortic root (Figure 13). In this design, the force transducer's output measurement depends on its geometry because essentially, it acts as a strain gauge. Therefore, the force output depends on the strain experienced by the gauge, which itself depends on the geometry of the gauge. As such, the force measured by the force transducer as applied in [6] is not actually a quantity which is intrinsic to the aortic root itself.

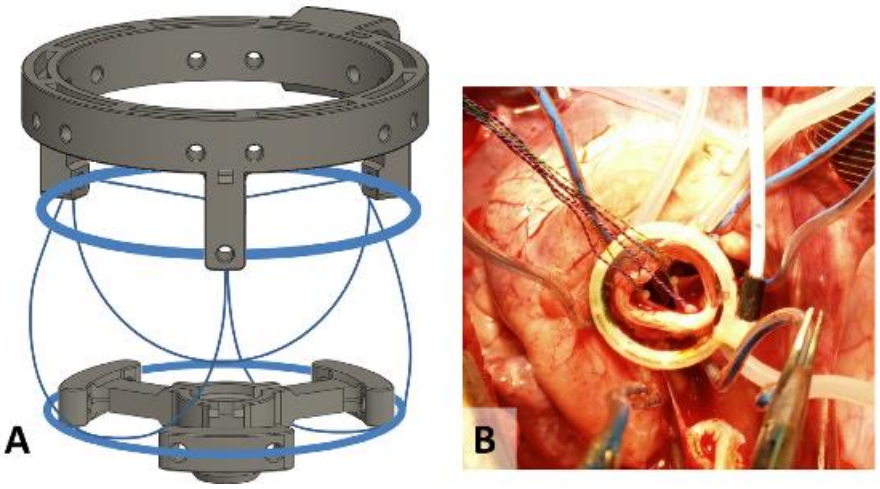

Figure 13: (A) Location of Force Transducers in the Aortic Root (B) In-vivo Image Showing STJ Transducer Implanted at Aortic Root [6]

2.6 KNOWLEDGE GAP

Although a prototype handheld measurement device for the AV was available at the University of Ottawa, it was not understood how well this device performed as only a cursory test of concept had been carried out. Consequently, it was necessary to determine the efficacy of the device, as well as the next steps for further development.

The measurement device was tested on three aortic pig valves at the University of Ottawa Heart Institute (UOHI). The goal of the experiment was to determine the accuracy of the device, along with the interobserver and intraobserver reliability of the measurements, because different users might use the device differently. Three specific measurements were made on each aortic pig valve using the device and these measurements later allowed for the calculation of the STJ diameter of the valve and the cusp free margin length and height (this will be explained in detail in Chapter 3). To compare these prototype-derived measurements to the "ground-truth" dimensions of the AVs in diastole, 3D images of the AV under 80 mmHg static pressurization were obtained using an ultrasound machine with the help of Dr. Benjamin Sohmer, echocardiographer at the UOHI. These images were analyzed to provide the "ground-truth" dimensions of the AVs.

A different but complementary line of inquiry that quickly presented itself was as follows: can point forces applied at certain locations in an unpressurized aortic root (as is accomplished by the prototype device) be used to recreate loading conditions and dimensions that occur when the valve is closed, under pressure, as in the end of diastole? If so, what are the direction and magnitude of such forces and what influences them? Finally, where exactly should they be applied? It is only when such questions have been answered that the ideas explored with the prototype measurement device may be thoroughly exploited. It is also important to evaluate whether several devices might be necessary (each one being designed for a certain force or valve dimension range).

3 EXPERIMENTAL TESTING OF MEASUREMENT TOOL PROTOTYPE

This section begins by introducing the prototype device by presenting diagrams and a free-body diagram to help the reader better understand the underlying mechanism of operation. Next, the theory based on solid mechanics, on which the prototype device was designed and manufactured, is presented. The experimental procedure is then presented including exactly how the prototype device was operated and what measurements were made from the device. Finally, a detailed explanation of the calculations necessary to obtain certain valvular dimensions is presented, followed by a discussion and conclusion of the results obtained from the experiment.

3.1 INTRODUCTION

A measurement tool in the form of a handheld device was designed using SolidWorks 3D modelling program [19] and then 3D-printed in several parts because of build-volume constraints. The choice of polylactic acid (PLA) as 3D-printed material made for a cheap and easy way to quickly produce and test a prototype. Finally, the device was assembled using off-the-shelf nuts and bolts of appropriate sizes. All this work was done at the University of Ottawa in Dr. Labrosse's laboratory before this thesis work started. The purpose of this prototype was to test the feasibility of intra-operative measurement of the AV component dimensions using controlled force application, while approximating the pressurized dimensions of the AV [18]. The inventor and co-inventor of the prototype are Dr. Labrosse and Dr. Dallard, respectively. Dr. Dallard was a former post-doctoral fellow in Dr. Labrosse's laboratory.

The prototype device (Figures 14 and 15) acts as a set of two perpendicular pliers which, when depressed, apply controlled forces onto specific locations of the unpressurized AV to approximate the physiological pressurized dimensions, and then allows for the measurement of the corresponding pressurized dimensions of the valve [18]. Split into three functional structures, the first structure of the prototype (shown in orange in Figure 14), is the holding end of the device and stays out of the AV during measurement [18]. It consists of the controlled force applicators which the user can press down to extend the blue and green prongs radially (Figure 14) [18]. It was designed so that when the force applicator is fully depressed (closing the gap between the

deflecting beam and its support), the user knows that the desired force is applied [18]. The set of green and blue prongs on the device are fastened to the first orange structure using nuts and bolts. These prongs allow for point force application to specific locations of the AV [18]. The first set of two prongs (shown in blue in Figure 14) are designed to extend the commissures of one AV cusp at a time. As such, they will be referred to as the commissure prongs. The second set of two prongs (shown in green in Figure 14) are designed to "stretch and span the distance between the middle of a cusp's free margin and the corresponding sinus of Valsalva (the attachment of the aortic cusp to the aortic wall)" [18]. They will be referred to as the cusp prongs. Finally, a slider (not shown) was designed to reach down to the lowest point of the valve's sinus being measured [18]. After both sets of the prongs are extended, a mechanism allows the user to lock them in position before the device is removed from the valve and the distances between the prongs measured using a Vernier caliper [18].

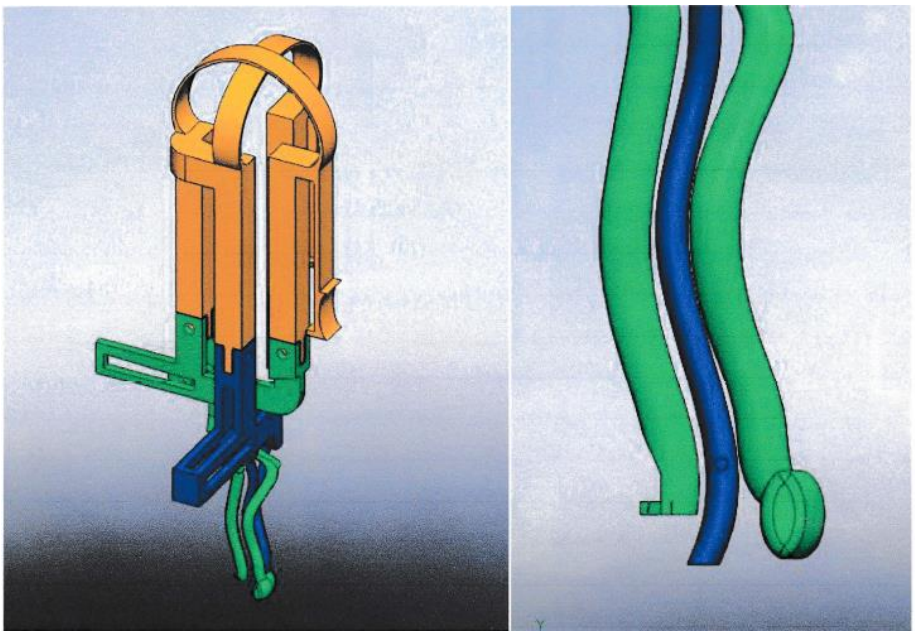

Figure 14: Prototype handheld AV measurement device with detailed view of Prongs [18]. See main text for explanations.

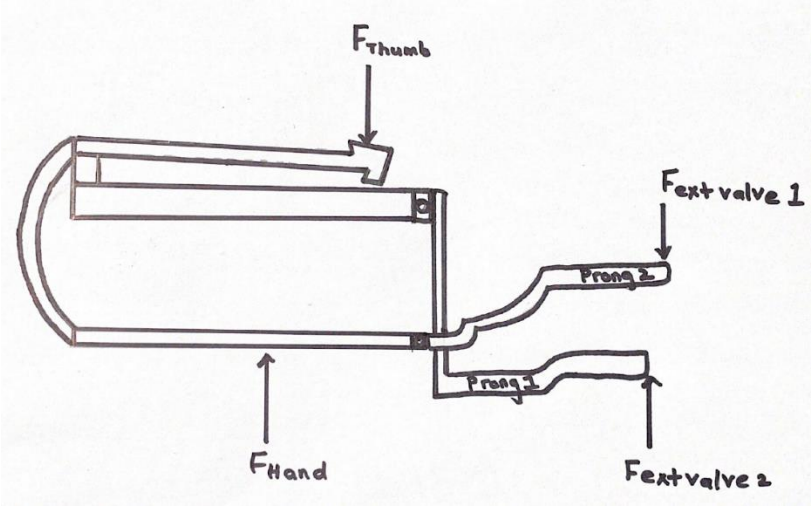

Figure 15: Free-body diagram depicting the mechanism of action of the prototype device. The user applies F_{Thumb} which allows Prong 1 to extend against a component of the valve cusp. F_{Hand} is the force exerted on the device by the user's palm during measurement. $F_{extvalve1}$ and $F_{extvalve2}$ are forces exerted on the device by the valve's cusp components.

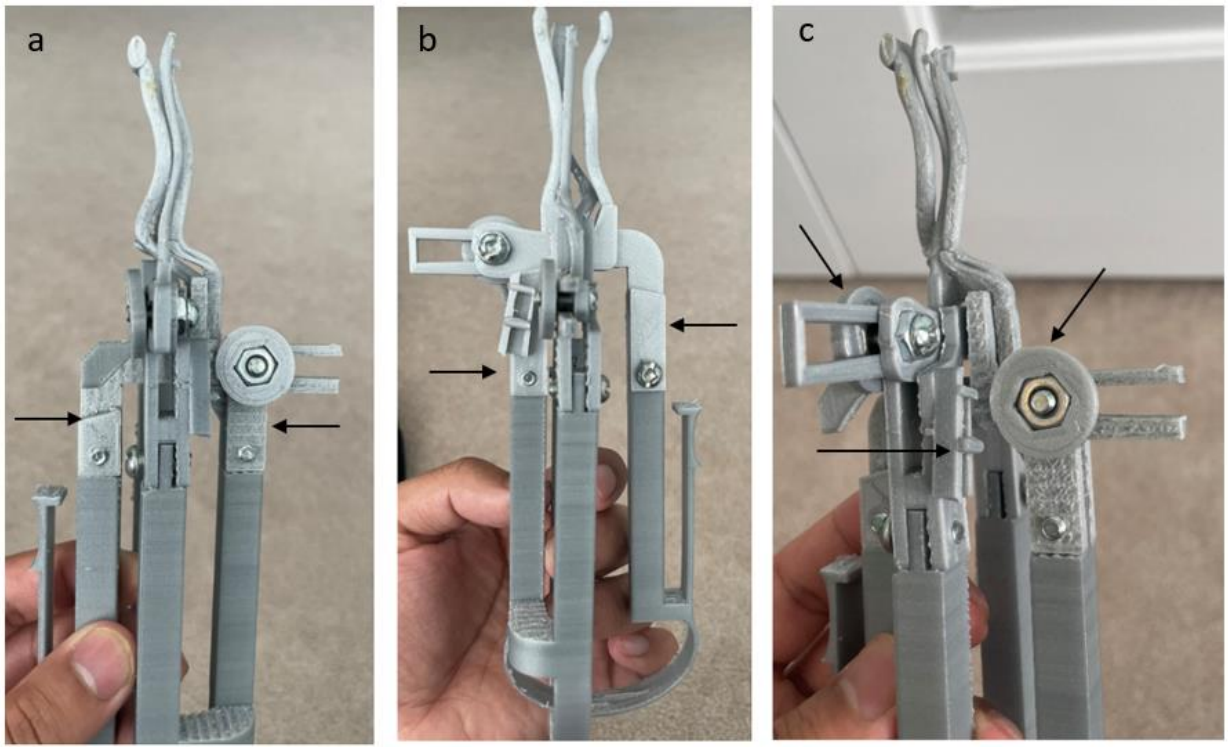

Figure 16: (a) Prototype with arrows pointing to two distinct parts that make up the cusp prongs. On the right is a fixed part, and on the left is the counterpart that can move in the same plane as the fixed part, along sliders. (b) Prototype rotated counter-clockwise 90 degrees from (a), with arrows pointing

to two distinct parts that make up the commissure prongs. On the left is the fixed part, and on the right is the counterpart that can move in the same plane as the fixed part, along sliders. (c) View showing the two rounded fixtures (right and left arrow) used to secure the position of the prongs. The arrow in the middle points to the guide for the slider (not shown) that is extended down to the lowest part of the valve's sinus.

The three cusps can be measured individually in sequence, using the same protocol. As will be detailed later, the measurements that can be obtained (directly or indirectly) by the prototype device include the distances between the valve's commissures, the STJ diameter, and the cusps' free margin length and height [18].

Before expanding on the testing of the prototype device, it is interesting to provide more details on the force-control mechanism around which it was designed. Indeed, the two perpendicular force applicators on the prototype were sized to achieve specific forces using the bending properties of thin beams. One of the force applicators from the prototype, as well as the approximately assumed location of force application, is illustrated in Figure 16. The force applicator was assumed to act as a cantilever beam under transverse point load. This applied load would cause the beam to deflect downwards from its natural position (as seen in the elastic curve category in Figure 17). According to linear elasticity, the deflection of the beam depends on Young's modulus of the material used, the moment of inertia of the beam, the magnitude of the force applied and the distance of the applied force from the fixed support [20]. For a simple cantilever beam set-up as depicted in Figure 17, the maximum deflection can be found by multiplying the force (P) by the cube of the length from the support (L) and dividing that all by three times the Young's modulus (E) and moment of inertia (I) [20]. It must be noted that in the analysis, several assumptions are made, including the beam being straight, linear elastic deformation, high length to height ratio and small deflections [20].

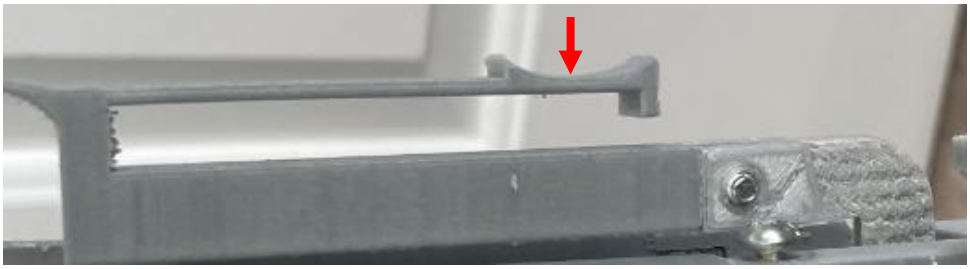

Figure 17: Photograph of a force applicator on handheld measurement device.

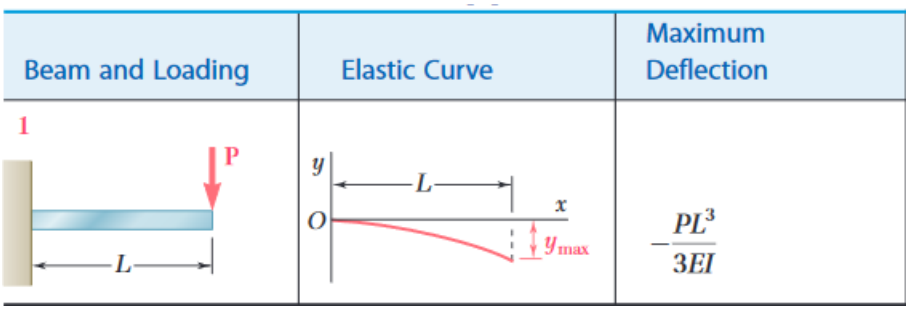

Figure 18: Maximum deflection for simply loaded cantilever beam [20].

Depending on what parameters are to be designed for, the other variables in the maximum deflection equation of the analysis (Figure 17) can be varied. For instance, if a certain force is chosen to be applied by the device, and the Young's modulus is known, the moment of inertia (which contains the dimensions of the beam) and the distance from applied force to the support (*L)* can be adjusted for optimal design. For the inaugural design of this prototype, a force of 1 N was arbitrarily chosen by the inventors.

When the user presses down the force applicator (Figure 16), it was assumed that all the force went all the way through to the prongs and was consequently experienced by the corresponding component of the AV. Any friction losses because of the two segments of the prototype sliding against each other (this was designed for lateral stability) were neglected as they were assumed to be small.

3.2 METHODS

The concept of the prototype was tested at the University of Ottawa Heart Institute (UOHI) using porcine AVs. Five pig hearts were obtained from an abattoir and kept in a freezer at the UOHI until the day of the experiment.

Two of the valves were unintentionally destroyed during the preparation and were therefore rendered unusable and thrown away. In the remaining three hearts, the ascending aortas were cut all the way down to a few centimeters above the STJ level. Thereafter, the ascending aortas were cannulated and connected to a static pressure head to pressurize the closed AVs to 80 mmHg pressure to simulate end-diastolic physiological pressure. Whilst under this pressure, a 3D transesophageal echocardiography (TEE) machine was used by Dr. Benjamin Sohmer to determine the true AV dimensions of each valve. These dimensions were considered as the "ground-truth" dimensions of the AV under closed end diastolic pressure. The goal of the experiment was to compare these "ground-truth" dimensions with the same dimensions obtained using the measurement prototype device.

The accuracy of the device was evaluated by comparing the measurements taken using the prototype to the "ground-truth" dimensions described above. The precision of the device was evaluated by having three people perform the same measurements on the same valves. A device with a high accuracy would theoretically yield measurements very close to those obtained from ultrasound imaging. On the other hand, a device with high precision would yield measurements taken by each observer (person measuring) that do not differ by much, on any one AV.

There were four participants who conducted the measurements using the prototype device: Dr. M. Guo (cardiac surgery resident), Dr. M. Labrosse, Dr. P. Thin Vo (cardiac surgery resident), and this thesis writer. Three rounds of measurements were performed on the first AV, as shown in Table 1.

Table 1: First AV experimental procedure

Round 1	Dr. Vo for device insertion with Ming for assistance, and Michel for measurements off digital caliper
	Dr. Guo for device insertion with Peter for assistance, and Michel for measurements off digital caliper
	Rohail for device insertion with Peter for assistance, and Michel for measurements off digital caliper
Round 2	Dr. Vo for device insertion with Ming for assistance, and Rohail for measurements off digital caliper
	Dr. Guo for device insertion with Peter for assistance, and Rohail for measurements off digital caliper
	Rohail for device insertion with Peter for assistance, and Rohail for measurements off digital caliper
Round 3	Dr. Vo for device insertion with Ming for assistance, and Rohail for measurements off digital caliper

Due to time constraints, the second and third valves were stored in 4^{o}C saline solution at the UOHI for one week, until the next series of measurements could be conducted. Two, instead of three rounds were conducted for the second and third AVs. The exact sequence can be seen in Tables 2 and 3:

Table 2: Second AV experimental procedure

Round 1	Dr. Vo for device insertion with Ming for assistance, and Rohail for measurements off digital caliper
	Dr. Guo for device insertion with Peter for assistance, and Rohail for measurements off digital caliper
	Rohail for device insertion with Ming for assistance, and Peter for measurements off digital caliper
Round 2	Dr. Vo for device insertion with Ming for assistance, and Rohail for measurements off digital caliper

	Dr. Guo for device insertion with Peter for assistance, and Rohail for measurements off digital caliper
	Rohail for device insertion with Ming for assistance, and Peter for measurements off digital caliper

Table 3: Third AV experimental procedure

Round 1	Dr. Vo for device insertion with Ming for assistance, and Rohail for measurements off digital caliper
	Dr. Guo for device insertion with Peter for assistance, and Rohail for measurements off digital caliper
	Rohail for device insertion with Ming for assistance, and Peter for measurements off digital caliper
Round 2	Dr. Vo for device insertion with Ming for assistance, and Rohail for measurements off digital caliper
	Dr. Guo for device insertion with Peter for assistance, and Rohail for measurements off digital caliper
	Rohail for device insertion with Ming for assistance, and Peter for measurements off digital caliper

To determine the dimensions of each cusp in the AV, the first step was to insert one of the commissure prongs down one of the commissures of a cusp, until the free margin of the cusp touched the small dowel protruding from the prong and marking the desired depth of insertion. Then, the opposite commissure prong was extended, and the controlled force applicator was fully depressed to apply the designed application force at the opposite commissure.

While holding the commissure prongs in the same configuration, the curved cusp prong was set against the sinus of Valsalva nearest the cusp of interest, and the opposite hooked prong was extended, and the controlled force applicator was fully depressed to apply the designed application force at the middle of the cusp's free margin (Figure 18).

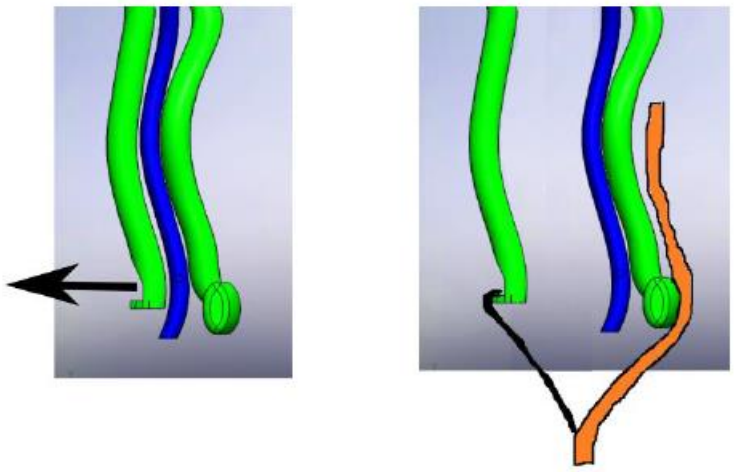

Figure 19: Extending the middle of the free margin on a single cusp [21].

When this was achieved, both sets of prongs were locked in place by tightening a wing nut on each set (Figure 15c).

Finally, a depth probe was slid down the sinus and cusp cavity until it reached the lowest point of the cusp where it attaches to the aortic wall (nadir), as can be seen in Figure 19. Once the depth probe was in place, it was clamped to the device and the device was removed from the valve for measurement.

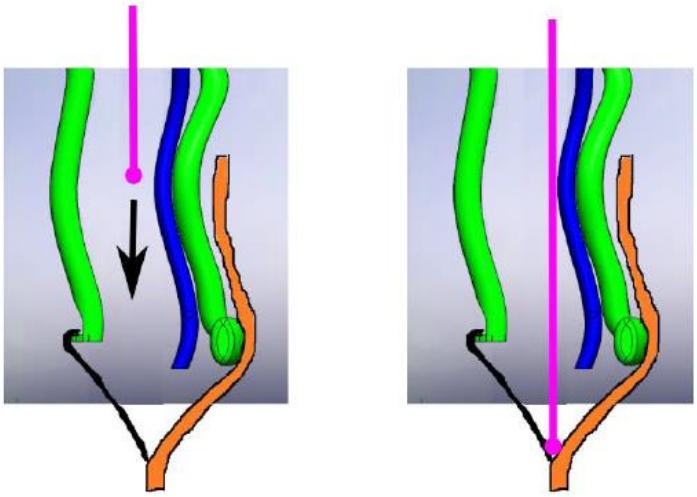

Figure 20: Inserting the depth probe to the lowest point of the cusp [21].

Each time the device was removed from the cusp being measured (three cusps in total for each AV), specific measurements were acquired from the device using a Vernier caliper. Firstly, the distance between the two locked commissure prongs were measured (Figure 20), the distance

between the locked curved probe and the hooked probe (Figure 21a) and lastly, the projected height between the nadir of the sinus and the middle of the free margin of the cusp (Figure 21b).

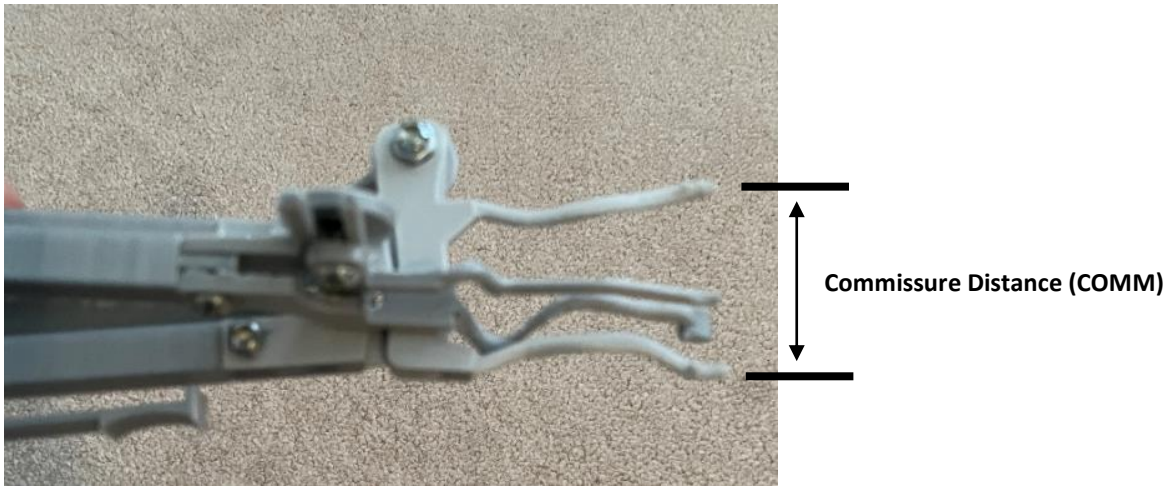

Figure 21: Measurement between two commissures.

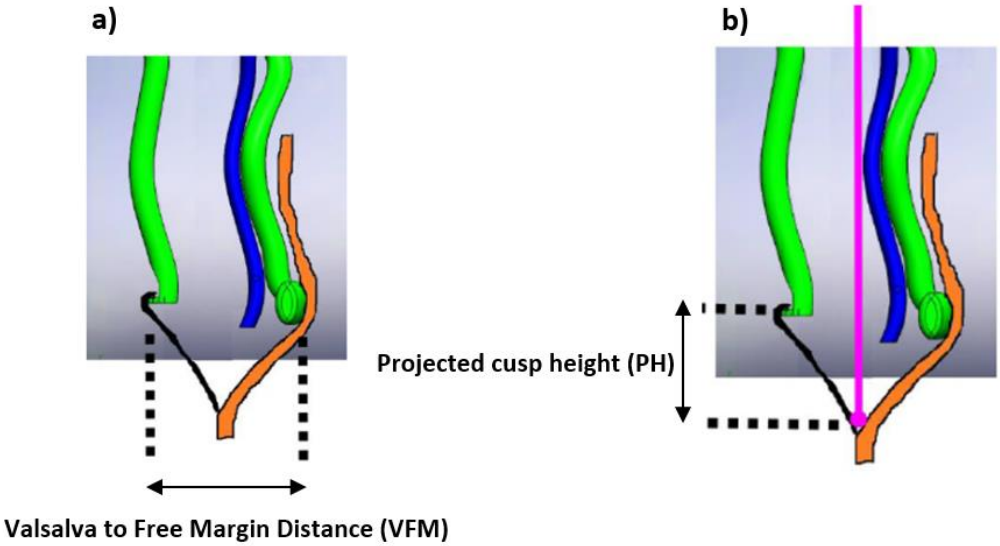

Figure 22 (a): Measurement between sinus of Valsalva and the middle of the free margin; (b): Measurement of projected cusp height [21].

Once the measurements of each porcine AV were gathered, calculations were conducted using a provided MATLAB script (Appendix A). The measured parameters from the experiment at the UOHI were the inputs of the program, and the outputs were the free margin and height for each cusp, and the STJ diameter for each valve, which were computed for each round of measurements described in Tables 1-3.

By design of the measurement device, the position of the commissure prongs relative to the cusp prongs was not adjustable. Indeed, the device was built to accommodate a range of dimensions found in normal AVs in adults. The determination of the free margin length and the height of each cusp was assisted by assigning, by design, appropriate distances DC and DS in Figure 23 in a typical AV cusp. Distance DC represents the distance from the middle of the free margin, when the AV is closed, to one adjacent commissure; distance DS represents the perpendicular distance from the middle of the free margin to the same commissure, again when the valve is closed, as seen in Figure 23. The manufacturing and design of the prototype device considered these distances and as such, DC and DS were constant values which were used for the calculations for each cusp in each valve. One of the assumptions when using this method to calculate the cusp dimensions was the user would first place the yellow and red prongs (Figure 22) on the commissure and sinus of Valsalva, respectively, for each cusp. This would be the initial configuration of the prototype before extending the prongs. The blue and grey prongs would then be extended using the force applicator to extend the other commissure and middle of the free margin, respectively, for each cusp (Figure 23). Another assumption is that when fully stretched, each cusp free margin length could be approximated as the sum of two straight-line distances, hence the two right-angle triangles seen in Figures 23 and 24. When broken down as such, and knowing the fixed distances DC and DS, and once the measured values COMM, VFM and PH are obtained (Figures 20 and 21), the values of the cusp free margin (FM) and cusp height (LH) could be easily calculated by using the Pythagorean theorem.

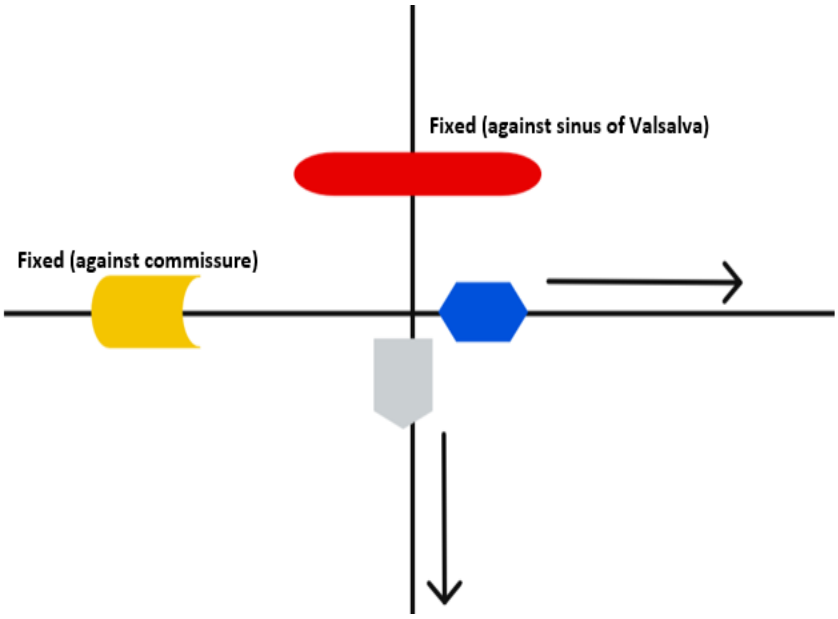

Figure 23: Initial configuration of device relative to positioning in AV cusp.

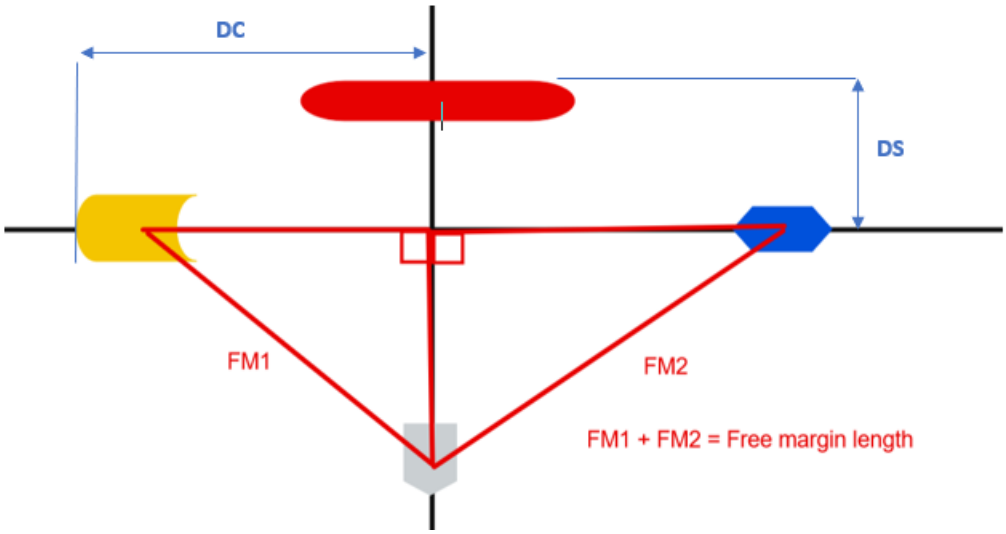

Figure 24: Extended configuration of device relative to positioning in AV cusp with fixed dimensions DC and DS, and right triangle approximations. See main text for details.

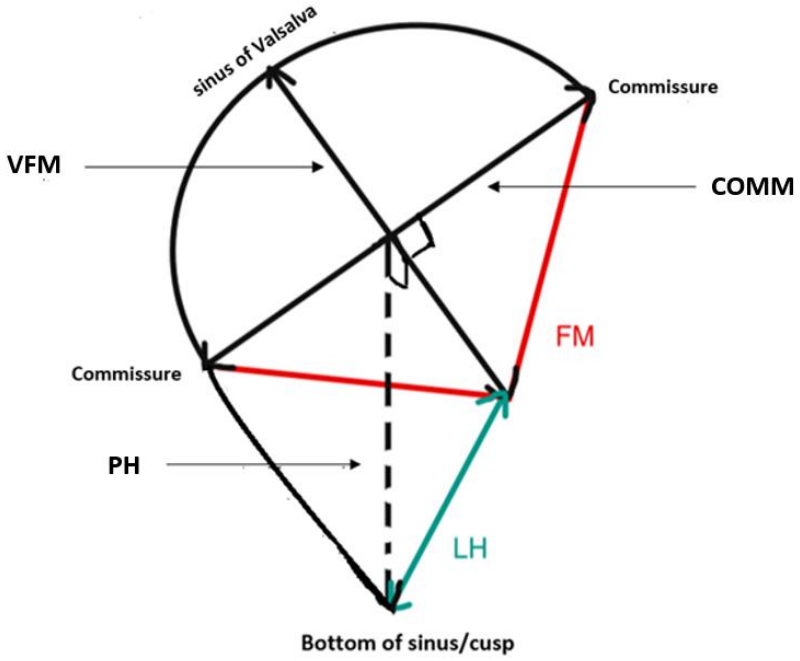

Figure 25: AV cusp dimensions estimations.

To calculate the STJ diameter of each of the AVs from the measurements acquired from the device, the STJ diameter was idealized as that of the circumscribed circle that passed through the three commissures of the AV (Figures 25 and 26). From Figure 26, the diameter of the circumscribed circle can be calculated by the following formula [22]:

$$diameter = \frac{abc}{2\ x\ area} = \frac{|AB||BC||CA|}{2\ x\ area} \quad \text{Eq. 1}$$

$$= \frac{abc}{2\sqrt{s(s-a)(s-b)(s-c)}}$$

$$= \frac{2abc}{2\sqrt{(a+b+c)(-a+b+c)(a-b+c)(a+b-c)}}$$

where a, b, c are the lengths of the sides of the triangle (the individual distances between two consecutive commissures) and s = (a+ b + c)/2 is the semi perimeter by Heron's formula and the expression $\sqrt{s(s-a)(s-b)(s-c)}$ is the area of the triangle, also by Heron's formula [22].

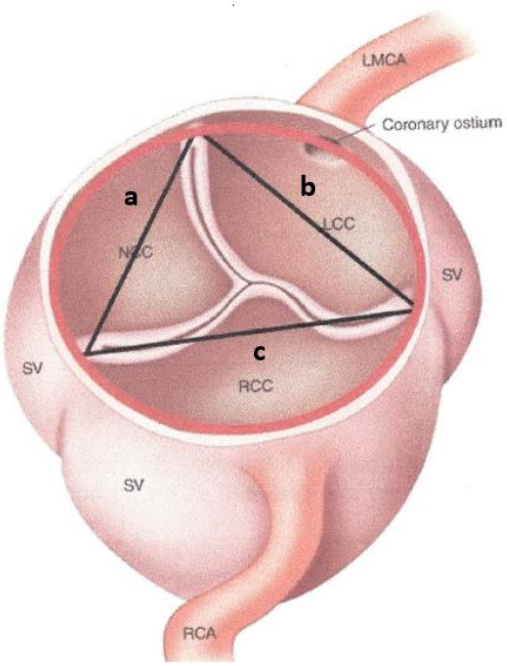

Figure 26: Approximation of AV STJ diameter as the diameter of the circle circumscribing the three commissures [23].

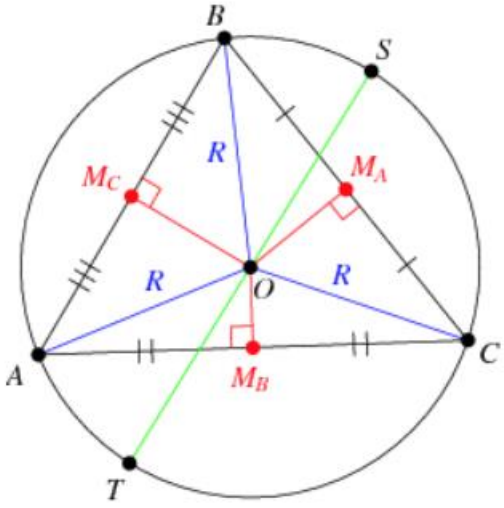

Figure 27: Depiction of a triangle with circumscribed circle [24].

Therefore, once the distances between all three commissures of the AV are known (lengths a, b, and c in Figure 25), the STJ diameter of the valve can be easily calculated. It is important to note that the method and technique for the above calculations for FM, LH and STJ was confirmed, analyzed, and consequently compiled by the author of this document, based on partial notes and drawings left by the inventors of the prototype.

3.3 RESULTS

Once all the raw measurements (distance between the commissures of each cusp, distance between the sinus of Valsalva and the middle of free margin, and the projected height of each cusp) were completed at the UOHI as explained above, the end results were tabulated (see Appendix B). Please note that in Appendix B, Com represents COMM, Vals represents VFM, and Height represents PH (Figure 21). Thereafter, a MATLAB script designed and provided by Dr. Labrosse (Appendix A), as mentioned above, was used to process the raw measurements, and calculate the corresponding cusp free margins and heights, and the STJ diameter of each valve. The results in millimeters (mm) are shown in Table 4.

In Table 4, NC, RC, and LC stand for non-coronary cusp, right coronary cusp and left coronary cusp of the valve measured, respectively. The last column shows the calculated average percent error between the "ground-truth" TEE dimensions obtained before starting the experimental measurements, and each of the measurements made on each of the three valves.

Table 4: Results of Experiments Conducted at the University of Ottawa Heart Institute. Dimensions in mm.

		Round 1			Round 2				Average
	AV ID	Dr. Vo	Dr. Guo	Rohail	Dr. Vo	Dr. Guo	Rohail	TEE	% Error wrt TEE
FM_NC	1	48.4	44.7	43.6	41.4	45.2	48.8	32.2	40.84
LH_NC	1	26.6	24.2	22.4	21.3	22.8	23.9	16.1	46.17
FM_RC	1	44.0	45.7	59.2	56.8	50.5	49.9	35.8	42.50
LH_RC	1	19.6	21.8	30.2	27.5	26.1	26.0	14.9	69.13
FM_LC	1	41.4	43.6	60.3	48.8	47.8	56.7	34.7	43.42
LH_LC	1	22.7	24	30	25.8	24.9	29.1	17.9	45.72
STJ	1	33.8	30.4	28	30.7	29.9	33.5	32.0	6.41
FM_NC	2	43.2	43.8	40.6	43.9	37.7	41.5	27.6	51.39
LH_NC	2	19.2	22.7	16.6	19.7	14.5	17.4	14.4	27.43
FM_RC	2	44.7	41.7	44.3	43.0	42.3	43.7	33.4	29.59
LH_RC	2	21.8	20.5	21.0	19.1	20.6	19.7	22.6	9.51
FM_LC	2	43.7	46.3	49.7	44.4	46.1	36.8	28.9	53.98
LH_LC	2	21.4	24.0	24.0	21.3	22.9	17.1	19.1	17.54
STJ	2	30.7	26.7	31.8	32.7	28.9	32.3	28.5	9.18
FM_NC	3	40.8	42.3	32.4	46.5	39.0	48.3	25.5	62.94
LH_NC	3	23.4	22.0	16.1	22.2	23.3	23.4	16.5	32.53
FM_RC	3	48.5	41.9	43.9	51.4	47.7	43.4	22.6	104.13
LH_RC	3	22.9	22.6	20.4	24.6	23.4	22.4	14.8	53.49
FM_LC	3	47.7	41.7	43.0	48.4	51.1	43.9	27.8	65.35
LH_LC	3	24.4	22.5	21.2	24.1	26.3	21.2	14.7	58.39
STJ	3	29.1	25.9	30.5	32.0	28.6	32.2	24.3	22.29

3.4 DISCUSSION AND CONCLUSION

If the measurement tool is eventually to be used by surgeons performing AV repair, it needed to be tested to determine its accuracy. From a practical perspective, and according to input from cardiac surgeons, the measurements obtained by the measuring tool should be within $\pm$ 2 mm of the measurements obtained by ultrasound imaging. Any error much greater than this may justifiably compromise the competence of the valve because it will not ensure the much needed geometrical accuracy of cusp coaptation. The results obtained by manual measurement using the device (as displayed in Table 4) featured an unacceptable overestimation of the "ground-truth" dimensions. Although some parameters were more promising than others (STJ for Valve 1, LH_RC and STJ for Valve 2), the force applied by the two force applicators on the device was likely too large to reproduce pressurized dimensions in the AV.

Testing of the prototype measurement tool confirmed the assumption that it would be feasible to apply controlled forces at specific locations in the unpressurized AV, although use of the prototype was awkward given the need to keep the force applicator fully depressed to ensure that the designed force was applied. However, testing of the prototype prompted two related questions: 1) could the application of smaller forces improve the accuracy of the tool? and 2) using the idea of controlled forces applied in specific locations of the unpressurized AV, is it possible to achieve a measurement accuracy within 2 mm? These questions led to changing the approach from experimenting with real AVs, to experimenting with computer models of AVs, as discussed next.

4 COMPUTER SIMULATION STUDY

This section begins by explaining and introducing the finite element (FE) software (LS-DYNA) in which the simulation study was carried out. Furthermore, this section also introduces the reader to the background on the FE method. Next, details are presented on how the simulation was run, namely what boundary conditions were applied to the FE model. Results of the simulation study are presented in figures and tables, followed by a discussion and conclusion on the findings.

4.1 INTRODUCTION

The experiments conducted on porcine AVs made it clear that a trial-and-error approach to fine-tune the forces applied by the measurement tool was required. However, iterating physical prototypes would require more 3D printing, which is not difficult; however, the preparation and testing of porcine AVs can prove challenging. This process is time consuming for everyone involved, and to further complicate things, access to clinical imaging equipment at the Heart Institute is very limited (even pre-pandemic). In this context, computer simulation was used to further investigate the forces experienced by the AV components under diastolic pressure. This was the obvious choice, especially as Dr. Labrosse's laboratory had already developed advanced computer models of AVs using real patient data from clinical imaging, as mentioned in Chapter 2. These models were already available to perform investigations and manipulations as will be presented below.

Before describing modelling further, let us briefly introduce finite element analysis (FEA). FEA is commonly used in lieu of physical prototypes to save time and money while allowing for optimization in design [25]. Many complex physical phenomena such as structural design, fluid behaviour or thermal flow, are described mathematically using partial differential equations (PDEs). FEA takes advantage of computers to solve these complex PDEs numerically providing the user with a better understanding of the stresses and strains and other quantities of interest to estimate the behaviour of a solid structures under given loads [25]. As an illustration, Figure 27 shows the stress distribution of an FEA simulation in a piston rod.

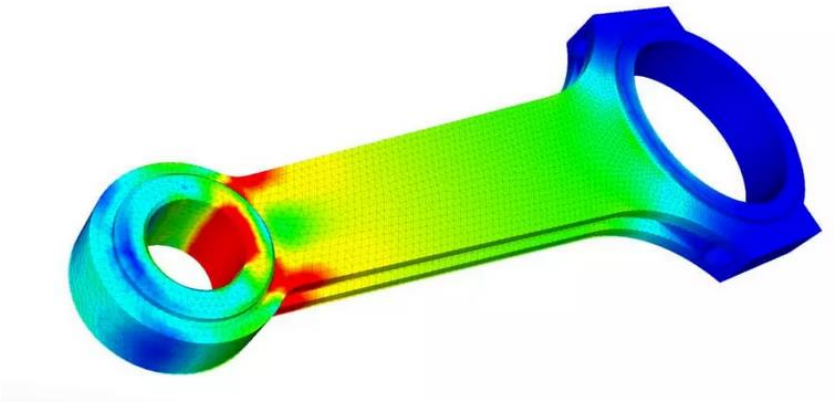

Figure 28: An example of results from an FEA analysis of a piston rod [25].

In a structural analysis, FEA requires the structure to be discretized (meshed) into elements of simpler shapes that are defined mathematically (e.g. hexahedra in 3D, or quadrilaterals in 2D). The elements are connected to each other through nodes. The elements are assigned material properties. Boundary conditions (how the structure is held in position) and loads need to be imposed before nodal displacements can be solved for by FEA. Further mathematical processing of the nodal displacements yields the strains in the elements, form which stresses can be determined. Mesh convergence, or "how small the elements need to be to ensure that the results of an analysis are not affected by changing the size of the mesh", is important in FEA [25]. Practically, if subsequent mesh refinements show no substantial change in the stress results, then the results can be assumed to have "converged" [25].

As explained in the literature review in Chapter 2, a "framework to process subject-specific 3D+t TEE AV data, determine the age matched properties for the aortic and leaflet tissues, build a finite element model of the unpressurized AV, and simulate the AV function throughout a cardiac cycle [10]" was developed and validated in Dr. Labrosse's laboratory. Namely, 3D+t TEE imaging datasets of human valves were processed in AVQ and simulated in AVSim to create FE models of different AVs. AVSim uses age-matched material properties of the aorta and the aortic leaflets, as explained in Chapter 2. AVSim then "iteratively scales the AV's unpressurized dimensions and drives the analysis of its dynamic mechanical behaviour during a cardiac cycle until the AV dimensions in late diastole match those measured by AVQ with a few percent error" [10]. The

method was validated by the close agreement between the dimensions in AVQ and AVSim, with a mean difference of 0.4 mm in 10 normal human valves [10]. Several dimensions of the AV were compared including the STJ diameter, and the cusps' free margins and heights [10]. Mesh convergence aspects were also considered.

As a result of this previous work, for the present simulation exercise, FE models of unpressurized human AVs were available for numerical investigation, along with their age-specific material properties. Figure 28 shows an example of an FE model of an unpressurized AV, with the sinuses of Valsalva and the ascending aorta removed to show the AV cusps. This model approximates well what a surgeon would see during AV repair.

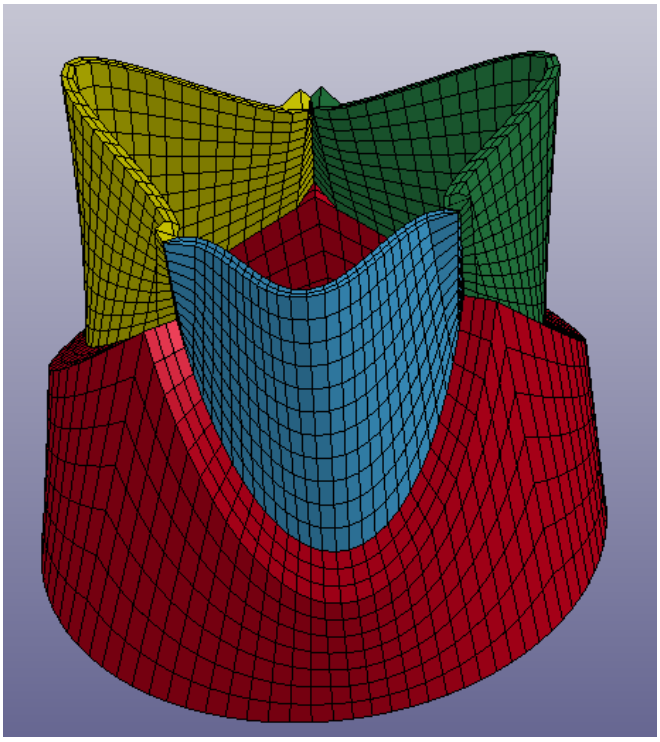

Figure 29: Finite element model of an AV as produced by AVSim.

To be clear, the present work took these FE models as starting points and was not concerned with how they were built. Of significance here is that these models provided validated in-silico human AV models that could be experimented on to hopefully glean the information needed to improve on the design of the AV measurement device.

For the purpose of this research, displacements or forces could be applied at specific locations on each cusp (shown in Figure 28 in yellow, blue, or green) to approximate how they would be applied

by the measurement tool. The resulting dimensions of cusp free margin lengths, cusp heights, and STJ diameter could easily be obtained from the analysis. In addition, since 3D+t TEE imaging data were available for these AV models, and provided their end-diastolic dimensions, the "ground-truth" target values for the pressurized dimensions were also known. Different displacements and forces could be tried on the FE models until the AV dimensions obtained from the simulations agreed with those from TEE imaging within an acceptable range. Of course, humans do not all have AVs with the same dimensions and shapes. To enrich the design space, the ten normal valves dataset reported on in [10] was complemented by two diseased human valves with severe AI. The type and level of forces or displacements necessary to obtain end-diastolic valve dimensions was meant to provide crucial information to adjust or redesign the measurement device.

4.2 METHODS

In keeping with the previous work, where AVQ and AVSim were coded in MATLAB [26], the FE simulations were run in LS-DYNA [27], and the results were gathered by LS-PrePost and processed through MATLAB. MATLAB was used to build the input deck for LS-DYNA.

After unsuccessful attempts to apply displacements and obtain the corresponding forces from the model, point loads (i.e., forces) were applied to the commissures of the valves and the middle of the free margins of the cusps. In Figure 29, the top of the commissures of the valves are represented by Nodes 2940, 2632 and 2324, while the middle of the free margins are represented by Nodes 12688, 11797 and 10906. Note that these nodes in the FE model are approximately where the prongs of the prototype were designed to apply point forces. Also note that, thanks to the systematic FE mesh construction in AVSim, the node numbering stays consistent with respect to location, in all the different valve models. To mimic the closure of the AV in diastole, the middle of the free margin of each cusp was to be pulled inward, while the commissures were pulled outwards. In LS-DYNA, point loads are defined using a node of application, a vector for direction, and a value for the magnitude of force as a function of time, input as a load curve. This was coded accordingly in the MATLAB code (Appendix C) generating an input deck for LS-DYNA.

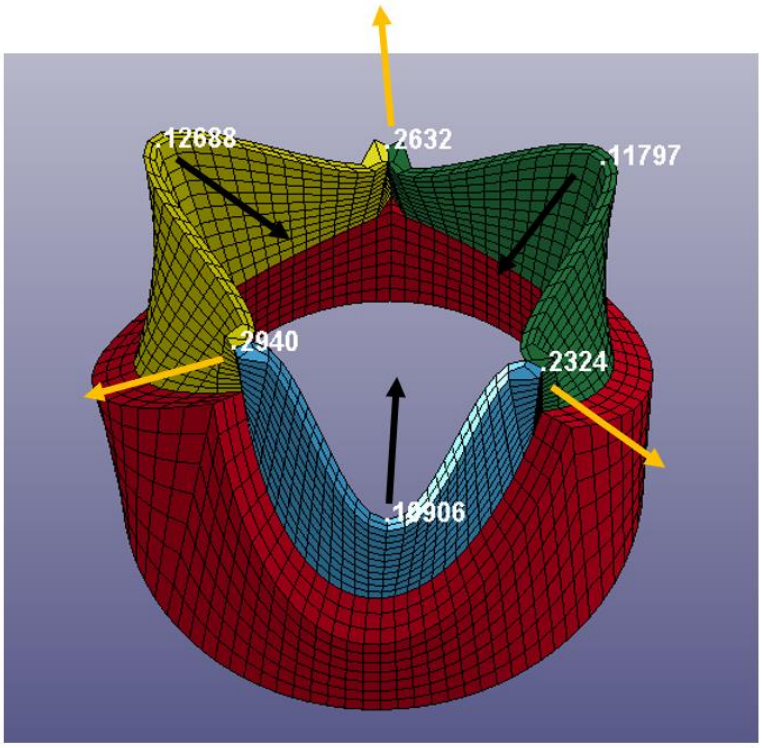

Figure 30: Finite element model of an AV in LS-DYNA showing the direction of point loads applied at the specific nodes indicated.

A commissure (see for example Node 2940 in Figure 29) will distribute forces toward its two adjacent cusps (the blue and the yellow cusps in Figure 29), along directions that extend from one commissure to the next. To account for this, two direction vectors were defined, and the resultant of these two was used as the direction for the applied force. For example, for the resultant force vector to be applied at Node 2940, a unit direction vector was created in the direction from Node 2324 to Node 2940, and another was created in the direction from Node 2632 to Node 2940. These two unit direction vectors were then summed to obtain the resultant unit vector defining the direction, along which the force at the commissure was applied. The exact same process was repeated for the other two commissures of the valves, namely at Nodes 2324 and 2632. The resultant vectors are displayed in orange in Figure 29.

The directions of the radially inward forces to be applied at the middle of the cups' free margins (purple dots in Figure 30) were assumed to lie in the plane containing the three middles of the cusp free margins. The centre of the circle circumscribing all three middles of the free margins was computed (red cross in Figure 30). Thereafter, unit direction vectors were defined from this centre point to each middle of the free margin. For example, for the blue cusp in Figure 29, the direction vector was created from Node 10906 to the coordinates of the centre point of the circumscribed circle. Two further unit direction vectors were constructed for the other two middles of the free margins, namely Nodes 11797 and 12688. This completed the creation of direction vectors that would allow for an approximate description of how each point on the AV cusps would be loaded in the simulation to represent point loads applied by the measurement device in porcine or human AVs.

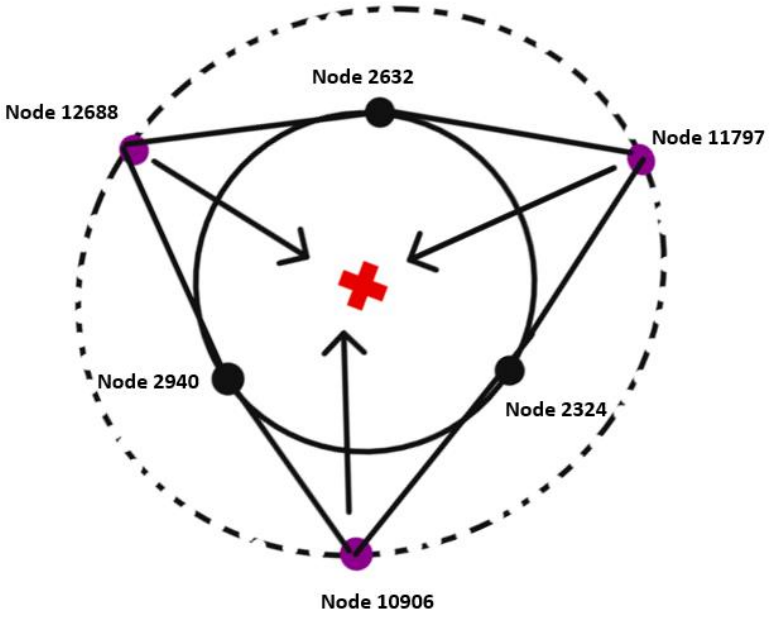

Figure 31: 2D Schematic of a bird's eye view of the FE model in Figure 27 of an AV in LS-DYNA. The outer dotted circle represents the circle circumscribing the three middles of the free margins of the valve cusps. The inner solid circle represents the circle circumscribing the three commissures of the valve. The red cross represents the centre point of the outer dotted circle, and the arrows pointing inward from the purple dots show the direction of application of forces on the middles of the cusps' free margins.

Note that, contrary to what was done in the experimentation at the Heart Institute (see Chapter 3) all three cusps of the AV were loaded simultaneously through the application of point loads, as an ideal measurement device would allow. Indeed, as the AV closes and opens in unison within the

human body, all three AV cusps needed to be loaded at the same time to approximate the physiological end-diastolic dimensions.

The goal of the simulation study was to apply forces at each of the six nodes as explained above and try to achieve AV dimensions, namely the STJ diameter, and the cusps' free margin lengths and heights that agreed with the end-diastolic dimensions measured from clinical imaging (i.e., in vivo). This was done through trial-and-error, by applying forces, letting the simulation run, and thereafter, post-processing the results to extract the AV dimensions obtained from LS-DYNA and comparing those to the dimensions obtained from the TEE imaging. Practically, the simulations were performed until the dimensions agreed within 2 mm of those obtained from TEE imaging. To start the simulation trial-and-error, the value of the forces were arbitrarily chosen to be 0.50 N at each commissure and each middle of the free margin. As more and more simulations were run, the values at any one of these six nodes on the model of the valve could be fine-tuned and adjusted to ultimately obtain a better agreement. This process was repeated for a total of twelve human AVs, for which TEE imaging data and the FE models were already available. The corresponding MATLAB code for the methods explained in this section can be found in Appendix C.

It is important to note that although the FE models created via AVSim were originally designed to simulate cardiac cycles (therefore dynamic behaviour), the present simulations were conducted in the quasi-static application of point loads. Therefore, the boundary and loading conditions only consisted of the following: all nodes at the bottom of the valve model were fixed, and ramp-like load curves for the point loads were applied within a short period of time (namely, 0.004 seconds, although the duration did not affect the results).

The post-processing module of LS-DYNA, LS-PrePost, was coded to extract the coordinates of specific nodes in the model at the end of each simulation. Namely, coordinates of the nodes at the commissures were tracked, along with those of the nodes along the cusp free margins, and those of the nodes along the cusp midlines, from the cusp nadir to the middle of the cusp free margin, on the ventricular side of the cusp. The node coordinates were saved to files which were further processed using a MATLAB code to compute the commissure-to-commissure distances, from which the STJ diameter was determined, along with the curvilinear lengths of the cusps' free margins and heights. The values were compared to their counterparts measured from clinical

images in end-diastole to evaluate the extent of the agreement, and iteration was performed on the force definition and application if necessary.

While conducting the simulations, it was noticed that it was difficult to obtain a good agreement for all the valve dimensions at once, a pattern noticed on all the 12 valves which were tried. However, it was noticed that a good agreement in any of the twelve tested valves could be achieved either for the STJ diameter and the cusp free margin lengths, or for the cusp heights, but never all three together. Although not an ideal situation, it was then decided to try for two cases: the first being agreement of the AV STJ diameter and cusp free margin lengths (Case 1), and the second, agreement of the cusp heights (Case 2). In other words, simulations were run for each of the twelve AV models that were available, by applying point loads to each of the six points of the valve (as described above) until the STJ and the free margin lengths of the cusps agreed with the TEE imaging dimensions within 2 mm. The process was then repeated for the same valves, but this time until the simulated dimensions agreed with the TEE dimensions for the cusp heights. Once satisfactory agreement was achieved, the corresponding forces and dimensions were recorded for both cases on each valve for further analysis.

Multiple linear regression analyses were carried out with MedCalc software (MedCalc, Version 19.7.4 for Windows, www.medcalc.org) [28]. A p-value of 0.05 or lower was considered to be statistically significant.

4.3 RESULTS AND PRELIMINARY INTERPRETATION

For each case, and for each valve, the commissural forces necessary to reach a satisfactory agreement with the TEE imaging dimensions were averaged. This was also done for the forces applied to the middle of the cusp free margins. Therefore, for each valve, there were four final force values, two for each case. For Case 1, the average forces at the commissures and the middle of the cusp free margins are noted FC_SF and FM_SF, respectively (Table 5). For Case 2, the average forces at the commissures and the middle of the cusp free margins are noted FC_L and FM_L, respectively (Table 6).

Table 5: Case 1 - Average force values at the valve commissures (FC_SF) and the middle of the free margins of the valve cusps (FM_SF) for satisfactory STJ diameter and cusp free margin lengths.

Valve ID	FC_SF	FM_SF
	Average ± SD (N)	Average ± SD (N)
1	0.40 ± 0.17	0.45 ± 0.05
2	0.48 ± 0.06	0.51 ± 0.07
3	0.40 ± 0.00	0.49 ± 0.13
4	0.39 ± 0.01	0.43 ± 0.08
5	0.17 ± 0.00	0.17 ± 0.03
6	0.41 ± 0.08	0.43 ± 0.03
7	0.20 ± 0.03	0.34 ± 0.05
8	0.65 ± 0.00	0.58 ± 0.04
9	0.50 ± 0.21	0.45 ± 0.04
10	0.43 ± 0.01	0.45 ± 0.09
AI3#	0.33 ± 0.06	0.21 ± 0.02
AI5#	0.33 ± 0.00	0.45 ± 0.14

Tables 6 presents the same data as Table, but for Case 2.

Table 6: Case 2 - Average force values at the valve commissures (FC_L) and the middle of the free margins of the valve cusps (FM_L) for satisfactory cusp heights.

Valve ID	FC_L	FM_L
	Average ± SD (N)	Average ± SD (N)
1	1.68 ± 0.68	0.01 ± 0.00
2	1.57 ± 0.51	0.14 ± 0.05
3	1.50 ± 0.36	0.19 ± 0.03
4	1.33 ± 0.65	0.18 ± 0.05
5	0.22 ± 0.04	0.18 ± 0.03
6	1.43 ± 0.20	0.11 ± 0.00
7	0.19 ± 0.04	0.36 ± 0.04
8	1.53 ± 0.06	0.29 ± 0.02
9	1.98 ± 0.88	0.07 ± 0.07
10	2.77 ± 0.34	0.07 ± 0.04
AI3#	1.00 ± 1.22	0.17 ± 0.07
AI5#	1.02 ± 0.18	0.27 ± 0.15

The data from Tables 5 and 6 were consolidated further with the standard deviation values removed as shown in Table 7. VAJ represents the ventriculoaortic junction diameter of each valve, STJ represents the sinotubular junction diameter, and H represents the height of the AV. The values reported for VAJ, STJ and H are the "ground-truth" measurements obtained from clinical imaging.

Table 7: Average force values (N) vs. "ground-truth" measurements for VAJ, STJ and H (mm).

Valve ID	Case 1		Case 2		VAJ	STJ	H
	FC_SF	FM_SF	FC_L	FM_L			
1	0.40	0.45	1.68	0.01	23.8	25.5	15.1
2	0.48	0.51	1.57	0.14	23.4	25.4	15.5
3	0.40	0.49	1.50	0.19	27.3	26.9	15.5
4	0.39	0.43	1.33	0.18	25.4	28.8	14.5
5	0.17	0.17	0.22	0.18	18.8	20.2	10.6
6	0.41	0.43	1.43	0.11	25.4	24.4	15.4
7	0.20	0.34	0.19	0.36	19.1	21.2	13.4
8	0.65	0.58	1.53	0.29	26.1	30.8	16.7
9	0.50	0.45	1.98	0.07	24.4	24.6	13.5
10	0.43	0.45	2.77	0.07	25.6	28.3	14.9
AI3	0.33	0.21	1.00	0.17	21.3	33.1	15.0
AI5	0.33	0.45	1.02	0.27	23.7	27.1	17.6

Multiple linear regression analysis was performed on all four of the average force values for each valve (FC_SF, FM_SF, FC_L, FM_L) individually (as dependent variable) against three independent variables VAJ, STJ and H. FC_SF, FM_SF, FC_L correlated very well with VAJ, exhibiting correlation coefficients of 0.73, 0.75 and 0.92, respectively (all with $p < 0.05$). On the other hand, FM_L did not correlate with any of STJ, VAJ or H.

Since three of the parameters (FC_SF, FM_SF and FC_FL) correlated very well with the VAJ diameter, it followed that, theoretically, several measurement devices could be designed for valves with different VAJ diameters, each device applying forces appropriate for the VAJ size range. However, it was noticed that, within the 12 valves tested, the force values for AVs with VAJ diameters between 24 and 28 mm were quite similar. As a result, in attempting to justify a single design for this range of VAJ diameters, analyses in LS-DYNA were run again on those valves with a VAJ diameter in that range (Valves 3, 4, 6, 8, 9 and 10) by averaging the force values in Table 7. The resulting averages were 0.46 N for FC_SF and 0.47 N for FM_SF in Case 1. On the other hand, the resulting averages were 1.76 N for of FC_L and 0.15 N for FM_L in Case 2. Since both

of these cases apply point loads to the same points in the AV during the simulation, both these sets of forces cannot be applied simultaneously. Thus, two separate loading cases need to be designed for, one to hopefully get satisfactory STJ diameter and cusp free margin lengths (Case 1) and another one to hopefully get satisfactory cusp heights (Case 2).

For verification, these two sets of forces were then applied to Valves 3, 4, 6, 8, 9 and 10 (valves with VAJ between 24-28 mm) at the appropriate locations to evaluate the theoretical accuracy of a prototype able to apply such forces. The resulting measurement errors in Cases 1 and 2 are shown in Tables 8 and 9, respectively. Note that the errors are in relation to the TEE "ground-truth" dimensions of each of the valves.

Table 8: Case 1- Errors on TEE dimensions

Valve ID	Errors (mm) in simulated dimensions wrt TEE dimensions			
	STJ	FE1	FE2	FE3
3	0.7 (+)	0.1 (+)	2.1 (+)	1.4 (-)
4	0.8 (+)	0.4 (+)	2.1 (+)	0.1 (-)
6	0.9 (+)	0.4 (+)	0.3 (+)	1.2 (+)
8	2.4 (-)	2.4 (-)	1.7 (-)	1.7 (-)
9	0.8 (-)	1.3 (-)	1.1 (+)	0.2 (-)
10	0.2 (-)	0.8 (-)	0.7 (+)	1.8 (+)

Table 9: Case 2 - Errors on TEE dimensions

Valve ID	Errors (mm) in simulated dimensions wrt TEE dimensions		
	LH1	LH2	LH3
3	0	0.8 (-)	1.5 (-)
4	0.6 (+)	0.3 (-)	0.6 (+)
6	0.4 (+)	0.5 (+)	0.1 (+)
8	1.4 (-)	0.8 (-)	0.6 (-)
9	2.5 (+)	0.2 (-)	0.4 (+)

As can be seen from Tables 8 and 9, there were three dimensions in Case 1 and one dimension in Case 2 that exceeded the acceptance criteria of a maximum difference of 2.0 mm (highlighted in yellow).

To try and further reduce these errors, a different analysis was attempted. This time, the STJ diameter of each valve (Valves 1-12) was plotted against each of the average force values for both cases, as can be seen in Figure 31. There are four data points (FC_SF, FM_SF, FC_L and FM_L) for each valve in Figure 31.

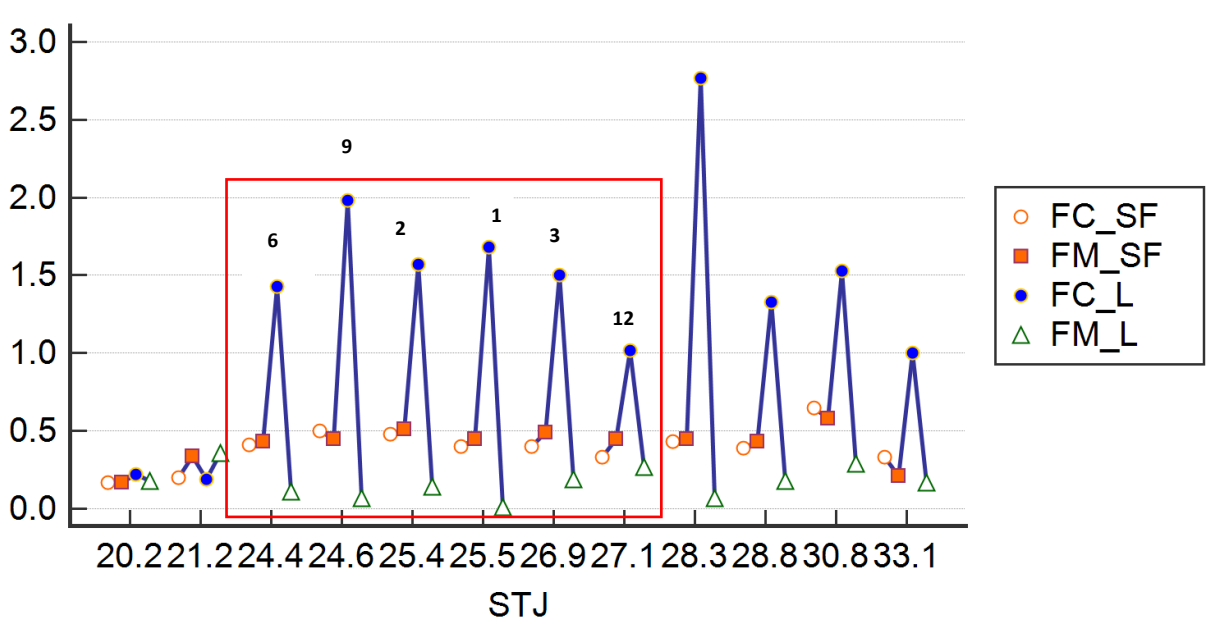

Figure 32: Clustered multiple variables graph showing relationship between STJ and FC_SF, FM_SF, FC_L and FM_L for all 12 AVs tested.

As can be seen from Figure 31, all four averaged forces (FC_SF, FM_SF, FC_L and FM_L) stayed in similar ranges for Valves 1, 2, 3, 6, 9 and 12 (labelled). Therefore, a cohort was made from these six valves and the average FC_SF, FM_SF, FC_L and FM_L was calculated which yielded 0.42 N, 0.46 N, 1.53 N and 0.13 N, respectively. Thereafter, as done before, these averaged forces were applied to Valves 1, 2, 3, 6, 9, and 12 twice (once for Case 1 and once for Case 2) to determine the accuracy of simulated dimensions under these loading conditions. The resulting measurement errors in Cases 1 and 2 are shown in Tables 10 and 11, respectively.

Table 10: Case 1 - Errors on TEE dimensions

Valve ID	Errors (mm) in simulated dimensions wrt TEE dimensions			
	STJ	FE1	FE2	FE3
1	0.8 (+)	0.7 (+)	1.9 (+)	0.5 (+)
2	1.2 (-)	0.9 (-)	0.0	2.0 (-)
3	0.3 (+)	0.3 (-)	1.7 (+)	1.6 (-)
6	0.4 (+)	0.1 (-)	0.0	1.0 (+)
9	1.4 (-)	1.6 (-)	0.6 (+)	0.5 (-)
AI5	1.3 (+)	1.3 (+)	1.0 (+)	1.5 (-)

Table 11: Case 2- Errors on TEE Dimensions

Valve ID	Errors (mm) in simulated dimensions wrt TEE dimensions		
	LH1	LH2	LH3
1	0.7 (+)	0.5 (+)	0.3 (+)
2	0.3 (-)	0.2 (-)	0.0
3	0.0	0.7 (-)	0.9 (-)
6	0.4 (+)	0.4 (+)	0.0
9	2.1 (+)	0.0	0.4 (+)
AI5	0.6 (+)	0.7 (-)	0.9 (-)

4.4 DISCUSSION

For almost all the valves that underwent testing by numerical simulation, the force at the commissures required to render agreement of the cusp height was greater than the force required to render agreement of the STJ diameter and the cusp free margin length together (Table 7). Furthermore, for most of the valves, the force required at the middle of the cusp free margin to render agreement of the cusp height was lower than the force required at the middle of the cusp free margin to render agreement of the STJ diameter and the cusp free margin length together (Table 7). This made physical sense because in Case 1, the commissures were not stretched as

much as in Case 2 (due to the lower applied point forces); however, on the other hand, in Case 1, the middle of the cusp free margins were pulled further in (due to the larger applied point forces) than in Case 2. This allowed for the agreement of the STJ diameter and the cusp free margin length of all the valves for Case 1. In Case 2 however, the point loads applied at the commissures were increased (Table 7), thus stretching the three commissures of the AV even more. This ultimately increased the STJ diameter of the valve. In addition, in Case 2, a decrease in the loading at the middle of the cusp free margins made it such that each leaflet was not extended inwards as much as in Case 1. This resulted in the reduction in the cusp heights. Ultimately then, the loading in Case 2 generally resulted in an increase in STJ diameter and a reduction in the cusp heights. It is because of these contradictory effects from point loads on the valve dimensions that an agreement could not be achieved for all the desired dimensions at once (STJ diameter, and cusps' free margin lengths and heights), a goal that was imagined at the beginning of the simulation study.

Valves 5 and 7 represented two anomalies in the data set. In Valve 5, FM_SF was lower than FM_L and in Valve 7, FC_SF was higher than FC_L, patterns that were opposite to those in the other valves. This was perhaps due the unique geometry of these patients' valves. Overall, though, certain loading conditions had positive effects on obtaining some of the AV dimensions, but simultaneously had a negative effect on other dimensions. Hence the decision to separate the experimentation and results into two scenarios (Cases 1 and 2).

As revealed from multivariable linear regression, FC_SF, FM_SF, and FC_L correlated well with the VAJ (atrio-ventricular) diameter, with correlation coefficients between 0.73 and 0.92. Since these correlation coefficients are close to the numerical value of 1, the independent and dependent variables are strongly correlated. In other words, there is a strong association between each of the valve's VAJ diameter and each of the applied forces (FC_SF, FM_SF and FC_L). Furthermore, the correlation between all these variables with VAJ was determined to be statistically significant ($p < 0.05$). This suggests that the two variables compared are indeed closely associated, and that the probability that they are so just by chance, is very small. As a result of these findings, it can be concluded that, in theory, different prototype devices could be designed for different AVs with different VAJ diameters. However, this poses an obvious practical concern, as no two AVs in humans are alike and designing a single device for each patient would prove impractical efficacy wise but also financially. However, it was noticed that certain valves out of the 12 tested had

remarkably similar values for the force required to achieve the pressurized dimensions (Table 7). Notably, Valves 3, 4, 6, 8, 9 and 10 had force values remarkably in the same range. Thus, these valves were grouped into a cohort for which a single prototype device could be designed. Note that this was arbitrarily done and any set of valves which had similar force values would most likely yield similar results. Valves 3, 4, 6, 8, 9 and 10 had VAJ diameter values between 24 mm and 28 mm. Consequently, a prototype device could be designed to treat patients with AVs with these VAJ diameters. This process could be repeated with valves of different sizes thus greatly reducing the number of devices needed. Finally, to determine the theoretical accuracy of a prototype that can be used in Valves 3, 4, 6, 8, 9 and 10, the forces for these valves were averaged and yielded average values for FC_SF, FM_SF, FC_L and FM_L. These forces were then applied to the FE models of Valves 3, 4, 6, 8, 9 and 10. It was determined that the results were unsatisfactory as the discrepancies with the ground-truth measurements exceeded the desired maximum 2 mm error range (Table 8 and Table 9), although many dimensions did agree to the accuracy requirement.

The results in Tables 10 and 11 (when the valves were grouped based on the STJ diameter) showed yet more accurate results compared to the results in Tables 8 and 9 when the valves were grouped based on VAJ diameter. Only one dimension in Case 2 (LH1 in Valve 9) did not meet the acceptance criteria of 2 mm by a small margin (0.1 mm). Regardless, the forces to be applied in Cases 1 and 2 being very different, one can anticipate the best accuracy from two different sizers (one for each case) to measure valves with an STJ diameter between 24 mm and 27 mm. Again, one device would allow for the accurate measurement of the STJ diameter and cusp free margin lengths (Case 1), while the other would allow for the measurement of the cusp heights (Case 2).

Conducting the simulation study revealed that it is indeed difficult to mimic the pressurization of the AV with just point load applications to specific locations on the valve. More specifically, it was determined that applying point loads to specific points to “pressurize” the valve does not correspond to the actual behavior and configuration of the AV in end-diastole. However, it was shown that the design of two different devices for AV measurement could achieve good accuracy for all the AV dimensions critical to AV surgical repair.

5 GENERAL DISCUSSION

5.1 DRAWING FROM THE CONCLUSIONS OF BOTH THE EXPERIMENTAL AND COMPUTER SIMULATION STUDIES

Given the results of the experimental measurements performed on porcine AVs, it was determined that the force (around 1 N) that the prototype measurement device was designed to apply to specific points on the AV was in fact too large. This was determined by comparison with ground-truth measurements obtained from TEE imaging, which included the cusp free margin lengths, the cusp heights and the STJ diameter. Indeed, the dimensions obtained from 3D-TEE imaging were generally smaller than those obtained by using the prototype measurement device. Therefore, this showed the necessity for a re-design or change in the approach to addressing the problem of intraoperative measurements of AV dimensions for AV repair.

From the numerical simulation study, it was shown that FE models of various AVs (normal and diseased) can be generated, then used to apply point loads at various locations of the valve and determine the response of the valve thereafter. More specifically, in this research, point loads were applied to various points on each of the AV cusps, namely approximately at the same locations at which forces would be applied with the measurement device prototype. The resultant dimensions in the valve after this applied loading were studied. Simulations of point load applications were adjusted until the resultant dimensions for various AV parameters (cusp free margin length, cusp height and STJ diameter) agreed with those deemed to be the ground-truth dimensions, within 2 mm. However, agreement of all dimensions at once could not be achieved, due to the complex interplay between these forces. For instance, if increasing certain forces yielded a better agreement for, say, the STJ diameter of the valve, the agreement for, say, the cusp height would become worse. This led us to shift our focus and to imagine two cases instead, one for matching one subset of AV dimensions, and another case for matching the remainder of AV dimensions of interest.

This research suggests that it is likely not possible to design just a single handheld measurement device to apply point loads, as they were applied in this research, to certain areas of the AV to simulate pressurized end-diastolic loading in the valve. However, if two measurement devices were acceptable, one could be designed for the measurement of the STJ diameter and cusp free

margin lengths of all the cusps in a valve, and another device could be designed for the measurement of all the cusp heights in the valve.

5.2 LIMITATIONS OF THE TECHNIQUES USED AND/OR CONCLUSIONS DRAWN

One limitation to this research involves the design of the inaugural prototype measurement device. Two dimensions (DC and DS, refer to Figure 23) were set as constants. These dimensions were implemented in the fixed components of the device and were used in the calculation of the aortic cusp dimensions. Although it is clear that the chosen dimensions for DC and DS were average values for a certain range of overall AV dimensions, no attempt was made to explore whether different values might be relevant for other ranges of AV dimensions, or whether individualized dimensions might actually be an absolute requirement. If the latter were to be the case, this would challenge the concept supported in this thesis that a finite number of measurement devices might be able to accommodate a wide range of AV dimensions.

Another limitation of the study is the proposed method to calculate the cusp free margin length and the cusp height from multiple dimensions measured by the device. It was assumed that the cusp free margin length could be represented as the sum of two straight-line distances when pressurized (Figures 23 and 24). This is a good approximation for the cusp free margin length when the cusp is in closed position (Figure 32) but introduced some minor error. The cusp height presents as more of a curved line in closed position in a real AV under pressure, but it was the goal of the hooked cusp probe of the device to apply a force that could reproduce the length of the physiological curved line along a straight line (Figure 32), and some minor errors due to right-angle triangle approximations used in the calculations can be expected. Still, because of the above-mentioned simplifications of the AV geometry, some error for the dimensions determined by the measurement device prototype was inevitable.

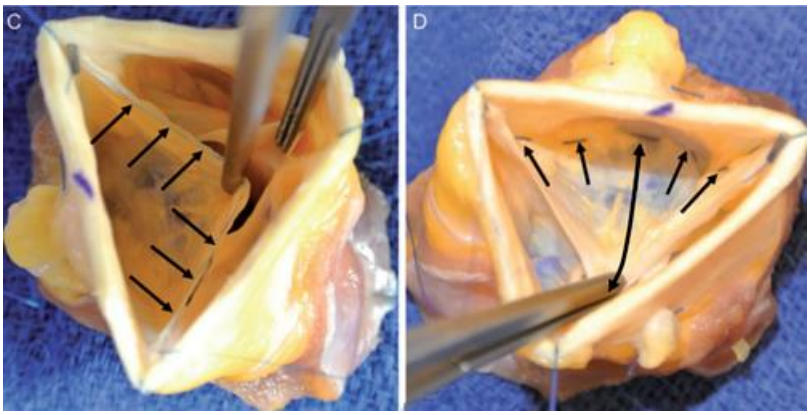

Figure 33: Photograph of an AV cusp being stretched into its approximate closed position by tweezers [8]. Left: the arrows are pointing to the cusp free margin length; right: the short arrows are pointing to the attachment line of the cusp, and the line with arrows shows the cusp height.

The prototype measurement device that was used in this research had been designed and manufactured within a couple of weeks at the end of Dr. Dallard's post-doctoral fellowship in Dr. Labrosse's laboratory, and as such, had not benefited from any testing or design iterations. Therefore, its precision and accuracy were first evaluated in the present work. After discovering that the forces that were being applied by the device were too large, computer simulations using finite element models of AVs were used to explore the types of forces that could be applied at specific points of the AV to replicate AV dimensions under pressurized conditions. However, when running these simulations, the way in which the forces were applied to the AVs was always consistent with how the forces would be applied by the prototype measurement device. This was a limitation in this research, as other directions and locations could have been explored.

6 CONCLUSION

6.1 BRIEF SUMMARY AND MAJOR CONTRIBUTIONS

A prototype measurement device had been designed and manufactured and was available at the start of the research. This device's intention was to allow surgeons to obtain measurements of the AV components during AV repair. In addition, these measurements were meant to approximate those in a closed and pressurized AV under end-diastolic pressure, thereby providing "in service" information.

The device was tested for its accuracy and precision using aortic porcine valves. 3D-TEE imaging was used to obtain "ground-truth" dimensions of three pig AVs under 80 mm Hg pressure. The prototype was used to apply point loads to artificially "pressurize" the aortic pig valves and obtain dimensions such as the cusp free margin lengths, cusp heights, and STJ diameter of the valve. The accuracy of the device was measured by comparing the dimensions obtained from 3D-TEE imaging with those obtained by using the device. The precision of the device was determined by comparing the dimensions obtained by three different users. In the end, however, precision concerns became futile as it was observed that the ground-truth dimensions of the AV were in fact considerably lower than those obtained by the device prototype, suggesting at minimum that the force it applied was too high, but also opening the possibility that the premise on which the prototype was based might be flawed.

A simulation study was therefore conducted to determine more precisely the point loads necessary to simulate pressurized conditions in an AV. This was done by using available finite element models of twelve human AVs, ten of which were normal (1-10) and two of which were indicated for aortic insufficiency (11 and 12). Point loads were applied to specific locations in these finite element models to replicate the type of loading exerted by the prototype. The goal was to use this loading method to try to replicate the end-diastolic (i.e., pressurized) AV dimensions.

The simulation work was conducted using a combination of MATLAB and LS-DYNA by modifying existing code and creating a few lines of new code where needed (an example is shown in Appendix C). From trial-and-error, it became apparent that, it was not possible to match all the desired valve dimensions at once. In other words, pressurized dimensions of the AVs could not be

replicated by just one measurement device. However, one could envision two devices tuned to different forces: one to measure the STJ diameter and the cusp free margin lengths, and another to measure the cusp heights, within 2 mm accuracy.

Overall, this research was able to propose a systematic and accurate method for the intra-operative measurement of AVs under conditions equivalent to the physiological (pressurized) state. This pressurized state is achieved by the application of carefully designed point loads to specific points of the AV. The approach more specifically provides dimensions for the cusp free margin lengths, the cusp heights, and the STJ diameter of the valve. As presented, the results of this research propose a system of two devices that would be accurate to within 2 mm for measurements in human AVs with sinotubular junction diameters between 24 mm and 27 mm.

6.2 RECOMMENDATIONS FOR FUTURE WORK

To fully exploit the ideas explored in this research, it is inevitable that further work is necessary. In particular, it would be beneficial to implement the forces required for agreement of the dimensions in both Case 1 (STJ diameter and cusp free margin length) and Case 2 (cusp height) in different designs of prototypes. This would allow for the validation of the results obtained in this research study. Furthermore, the design of the measurement device should be revisited to maximize ease of use, as the current prototype is quite bulky and awkward to use, hence posing an ergonomic challenge. If the validation and implementation of different prototypes proves successful, additional prototypes are recommended to be designed and tried to extend the range of valve dimensions that can be measured beyond those that are most critical for valve repair.

Lastly, it is recommended that any future researchers or collaborators on this project work very closely with cardiac surgeons for routine advice and consultation, from the preliminary design proposal all the way to the testing of any prototypes. This will ensure expert feedback can be obtained regarding the relevance and usability of the devices, thereby increasing the efficiency and quality of the final products.

7 REFERENCES

[1] AV regurgitation. (2020, August 07). Retrieved February 2, 2021, from https://www.mayoclinic.org/diseases-conditions/aortic-valve-regurgitation/diagnosis-treatment/drc-20353135

[2] Labrosse, M. R., Beller, C. J., Robicsek, F., & Thubrikar, M. J. (2006). Geometric modeling of functional trileaflet AVs: development and clinical applications. Journal of biomechanics, 39(14), 2665-2672.

[3] Labrosse, M. R., Beller, C. J., Boodhwani, M., Hudson, C., & Sohmer, B. (2015). Subject-specific finite-element modeling of normal AV biomechanics from 3D+t TEE images. Medical image analysis, 20(1), 162-172.

[4] Marieb, E. N., & Hoehn, K. (2019). *Human anatomy & physiology*. Hoboken, NJ: Pearson.

[5] Labrosse, M. (2019). *Cardiovascular mechanics*. Boca Raton, FL: CRC Press, Taylor & Francis Group.

[6] Bechsgaard, T., Hønge, J., Nygaard, H., Nielsen, S., & Johansen, P. (2017). Biomechanical assessment of the aortic root using novel force transducers. *Journal of Biomechanics, 61*, 58-64. doi:10.1016/j.jbiomech.2017.07.003

[7] Roberta Ancona, S. C. (n.d.). Epidemiology of AV stenosis (AS) and of AV incompetence (AI): Is the prevalence of AS/AI similar in different parts of the world? Retrieved from https://www.escardio.org/Journals/E-Journal-of-Cardiology-Practice/Volume-18/epidemiology-of-aortic-valve-stenosis-as-and-of-aortic-valve-incompetence-ai

[8] Labrosse, M. R., (2019). *A measurement device for a comprehensive approach to AV repair*. [Unpublished Powerpoint slides]. Cardiovascular Mechanics Laboratory, University of Ottawa.

[9] Labrosse, M. R., & Beller, C. J. (2007). AV leaflet sizer: a new device for AV sparing. *The Journal of heart valve disease*, *16*(2), 145–147.

[10] Labrosse, M. R., Beller, C. J., Boodhwani, M., Hudson, C., & Sohmer, B. (2015). Subject-specific finite-element modeling of normal AV biomechanics from 3D t TEE images. *Medical Image Analysis, 20*(1), 162-172. doi:10.1016/j.media.2014.11.003

[11] Martin, C., & Sun, W. (2012). Biomechanical characterization of AV tissue in humans and common animal models. *Journal of biomedical materials research. Part A, 100*(6), 1591–1599. https://doi.org/10.1002/jbm.a.34099

[12] Advancing 3D TEE. (n.d.). Retrieved April 7, 2021, from https://www.siemens-healthineers.com/ultrasound/news-and-innovations/advancing-3d-tee#chapter-block-3c21fb6765261647

[13] Schäfers, H. J., Bierbach, B., & Aicher, D. (2006). A new approach to the assessment of aortic cusp geometry. The Journal of thoracic and cardiovascular surgery, 132(2), 436-438.

[14] Labrosse, M. R., & Beller, C. J. (2007). AV Leaflet Sizer: A New Device for AV Sparing. Journal of Heart Valve Disease, 16(2), 145.

[15] Izzat, M. B., Hamzeh, K., Mahmoud, F., & Bakour, M. M. (2015). Aortic cusp sizers to establish the functional classification of aortic insufficiency: algorithm and midterm outcome of operative repair. Interactive cardiovascular and thoracic surgery, 21(1), 77-80.

[16] Dallard, J., Boodhwani, M., & Labrosse, M. R. (2018). AV Mechanics. Cardiovascular Mechanics, 279-318.

[17] De Kerchove, L., Momeni, M., Aphram, G., Watremez, C., Bollen, X., Jashari, R., ... & El Khoury, G. (2017). Free margin length and coaptation surface area in normal tricuspid AV: an anatomical study. European Journal of Cardio-Thoracic Surgery, 53(5), 1040-1048.

[18] Labrosse, M.R., Dallard, J., (2018). A hand-held device for the intra-operative measurement of AV components using controlled force application to approximate pressurized dimensions. *Invention Disclosure Form*

[19] 3D CAD Design Software. (n.d.). Retrieved April 7, 2021, from https://www.solidworks.com/

[20] Beer, F. P., Johnston, E. R., DeWolf, J. T., & Mazurek, D. F. (2015). *Mechanics of*

materials. New York: McGraw Hill.

[21] Labrosse, M.R., (2019). Prototype testing protocol.

[22] Circumradius. (n.d.). Retrieved February 8, 2021, from https://artofproblemsolving.com/wiki/index.php/Circumradius

[23] Themes, U. (2017, March 25). Ventricular Tachycardia and Cardiac Anatomy: Aortic Cusp. Retrieved February 8, 2021, from https://basicmedicalkey.com/ventricular-tachycardia-and-cardiac-anatomy-aortic-cusp/

[24] Circumcircle. (n.d.). Retrieved February 8, 2021, from https://mathworld.wolfram.com/Circumcircle.html

[25] What Is FEA: Finite Element Analysis? Documentation. (2021, January 20). Retrieved from https://www.simscale.com/docs/simwiki/fea-finite-element-analysis/what-is-fea-finite-element-analysis/

[26] MATLAB. (n.d.). Retrieved April 8, 2021, from https://www.mathworks.com/products/matlab.html

[27] DYNA. (n.d.). Retrieved April 8, 2021, from http://www.lstc.com/products/ls-dyna

[28] Schoonjans, Frank. "MedCalc Statistical Software - Free Trial Available." *MedCalc*, MedCalc Software, 5 Apr. 2021, www.medcalc.org/.

APPENDIX A

```
% measured data
% RC
Com_RC      =  22 ;
Vals_RC     =   17;
Height_RC   =   11;
% LC
Com_LC      =   27;
Vals_LC     =   21;
Height_LC   =   13;
% NC
Com_NC      =   30;
Vals_NC     =   27;
Height_NC   =   16;

% Fixed constant data from measurement device
DC          =   (12.1+13.2)*0.5; % along commissures length
DS          =   (9.9+10)*0.5; % along sinuses length

% RC cusps dimensions
FM_RC = sqrt(DC^2 + (Vals_RC-DS)^2) + sqrt((Com_RC-DS)^2 +
(Vals_RC-DC)^2)
EH_RC = sqrt((Vals_RC-DC)^2 + Height_RC^2)
% LC cusps dimensions
FM_LC = sqrt(DC^2 + (Vals_LC-DS)^2) + sqrt((Com_LC-DC)^2 +
(Vals_LC-DS)^2)
EH_LC = sqrt((Vals_LC-DS)^2 + Height_LC^2)
% NC cusps dimensions
FM_NC = sqrt(DC^2 + (Vals_NC-DS)^2) + sqrt((Com_NC-DC)^2 +
(Vals_NC-DS)^2)
EH_NC = sqrt((Vals_NC-DS)^2 + Height_NC^2)

% STJ
p = (Com_RC+Com_LC+Com_NC)*0.5;
S = sqrt(p*(p-Com_RC)*(p-Com_LC)*(p-Com_NC));
STJ = (Com_RC*Com_LC*Com_NC) / (2*S)
```

APPENDIX B

Peter				Round 1	Round 2	Round 3
AV ID	1	Cusp	Measure	Value	Value	Value
			Com	27.0	27.9	30.3
		NC	Vals	30.0	25.2	22.4
			Height	17.5	14.8	15.6
			Com	33.8	28.4	26.6
		RC	Vals	23.8	34.5	34.4
			Height	13.8	12.3	14.5
			Com	20.0	22.4	23.2
		LC	Vals	27.9	31.6	32.8
			Height	13.9	14.0	14.5

Ming				Round 1	Round 2	Round 3
AV ID	1	Cusp	Measure	Value	Value	Value
			Com	23.0	24.6	
		NC	Vals	29.1	28.9	
			Height	14.8	12.7	
			Com	29.4	25.6	
		RC	Vals	27.4	31.7	
			Height	13.0	14.5	
			Com	25.0	27.2	
		LC	Vals	27.8	29.6	
			Height	16.0	15.3	

Rohail				Round 1	Round 2	Round 3
AV ID	1	Cusp	Measure	Value	Value	Value
			Com	24.1	29.0	
		NC	Vals	28.1	29.5	
			Height	13.1	13.7	
			Com	25.0	28.2	
		RC	Vals	36.8	30.5	
			Height	13.8	16.0	
			Com	23.6	29.7	
		LC	Vals	37.7	34.0	
			Height	11.4	16.3	

Peter				Round 1	Round 2	Round 3
AV ID	2	Cusp	Measure	Value	Value	Value
			Com	28.3	29.4	
		NC	Vals	26.2	26.2	
			Height	10.2	11.1	
			Com	26.1	29.6	
		RC	Vals	28.1	25.5	
			Height	12.0	11.1	
			Com	24.9	25.6	
		LC	Vals	27.9	28.1	
			Height	11.6	11.2	

Ming				Round 1	Round 2	Round 3
AV ID	2	Cusp	Measure	Value	Value	Value
			Com	24.2	27.7	
		NC	Vals	28.2	22.7	
			Height	13.5	6.9	
			Com	24.2	24.8	
		RC	Vals	26.9	27.1	
			Height	11.5	11.4	
			Com	20.6	21.4	
		LC	Vals	30.6	30.3	
			Height	12.3	10.6	

Rohail				Round 1	Round 2	Round 3
AV ID	2	Cusp	Measure	Value	Value	Value
			Com	29.2	29.3	
		NC	Vals	24.0	24.6	
			Height	8.9	9.3	
			Com	27.3	29.7	
		RC	Vals	27.4	25.9	
			Height	11.7	11.5	
			Com	25.7	24.2	
		LC	Vals	31.2	23.8	
			Height	11.1	10.1	

Peter				Round 1	Round 2	Round 3
AV ID	3	Cusp	Measure	Value	Value	Value
		NC	Com	22.0	25.5	
			Vals	27.1	29.4	
			Height	15.9	10.6	
		RC	Com	28.1	30.6	
			Vals	29.7	30.5	
			Height	11.5	13.5	
		LC	Com	24.1	26.1	
			Vals	30.5	30.3	
			Height	12.7	13.0	

Ming				Round 1	Round 2	Round 3
AV ID	3	Cusp	Measure	Value	Value	Value
		NC	Com	22.6	25.8	
			Vals	27.8	24.6	
			Height	12.8	18.1	
		RC	Com	23.8	26.1	
			Vals	27.2	29.9	
			Height	14.6	12.2	
		LC	Com	20.4	21.8	
			Vals	28.0	33.0	
			Height	13.5	12.7	

Rohail				Round 1	Round 2	Round 3
AV ID	3	Cusp	Measure	Value	Value	Value
		NC	Com	26.3	28.0	
			Vals	19.4	29.6	
			Height	13.0	12.7	
		RC	Com	27.4	25.3	
			Vals	27.1	27.6	
			Height	11.0	13.8	
		LC	Com	25.4	29.8	
			Vals	27.3	26.0	
			Height	12.2	13.9	

APPENDIX C

```
fprintf(fid, '$---+----1----+----2----+----3----+----4----+----5----+----6----+----7----+----8\n');
fprintf(fid, '$                    BOUNDARY CONDITION CARDS\n');
fprintf(fid, '$---+----1----+----2----+----3----+----4----+----5----+----6----+----7----+----8\n');

% ***** BASE
% Preventing all displacements of all nodes on valve base
fprintf(fid, '*BOUNDARY_SPC_NODE\n');
fprintf(fid, '$ NID/NSID       CID      DOFX      DOFY      DOFZ     DOFRX     DOFRY     DOFRZ\n');
for i = 1:dim1
    fprintf(fid, '%10i %9i %9i %9i %9i \n',end1(i),0,1,1,1);     % no displacements in all directions
end
% Uncomment block below to prevent all displacements at the
% distal end of the ascending aorta
%{
for i = 1:dim2
    fprintf(fid, '%10i %9i %9i %9i %9i \n',end2(i),0,1,1,1);     % no displacements in all directions
end
%}

% ***** TOP
% Applying a longitudinal displacement to the distal end of
% the ascending aorta
%par.lambda = 1.30; % this overrides the value defined before
u = (par.lambda-1)*totH; % displacement
% LCID 1, VID 1
fprintf(fid, '*BOUNDARY_PRESCRIBED_MOTION_NODE\n');
fprintf(fid, '$      NID       DOF       VAD      LCID        SF       VID     DEATH     BIRTH\n'); % -4:
for i = 1:dim2
    fprintf(fid, '%10i %9i %9i %9i %9.4f %9i \n',end2(i),-4,2,1,u,1);     % -4,2 means no displacement al
end
% VID 1
fprintf(fid, '*DEFINE_VECTOR\n');
fprintf(fid, '$      VID        XT        YT        ZT        XH        YH        ZH\n');
fprintf(fid, '%10i %9.4f %9.4f %9.4f %9.4f %9.4f %9.4f\n',1,0,0,0,Zaxis(1),Zaxis(2),Zaxis(3));
% LCID 1: just a ramp from 0 to 1.0
fprintf(fid, '*DEFINE_CURVE\n');
fprintf(fid, '$     LCID      SIDR      SCLA      SCLO      OFFA      OFFO\n');
fprintf(fid, '%10i          %10.4f\n',1,1);
fprintf(fid, '$                A1                  O1\n');
fprintf(fid, '                  0                   0\n');
fprintf(fid, '%20f %19.9f\n', par.LSDtime(2),1.0);
fprintf(fid, '%20f %19.9f\n', par.LSDtime(time_max),1.0);

% ***** COMMISSURES
n1 = scaledLandmarks.U; % coordinates of Commissure 1
n2 = scaledLandmarks.V; % coordinates of Commissure 2
n3 = scaledLandmarks.W; % coordinates of Commissure 3

% Outward radial forces to be applied
force1 = 1.53; % Newtons
force2 = 1.53; % Newtons
force3 = 1.53; % Newtons
```

```
% Defining unit vector in global coordinate system
zu = [0 0 1]';

%--------- Commissure 1 -----------%
% Resultant unit vector at Commissure 1
R1 = (n1-n2)/norm(n1-n2) + (n1-n3)/norm(n1-n3);
R1 = R1/norm(R1);
% calculating unit vector x' in global coordinate system
xp1 = R1;
% calculating unit vector y' in global coordinate system
yp1 = -cross(xp1,zu);
yp1 = yp1/norm(yp1);
% CID 1
fprintf(fid, '*DEFINE_COORDINATE_SYSTEM\n');
fprintf(fid, '$      CID        XO        YO        ZO        XL        YL        ZL      CIDL\n');
fprintf(fid, '%10i %9.4f %9.4f %9.4f %9.4f %9.4f %9.4f %9i\n',1,n1(1),n1(2),n1(3),n1(1)+xp1(1),n1(2)+xp1(2),n1(3)+xp1
fprintf(fid, '$       XP        YP        ZP\n');
fprintf(fid, '%10.4f %9.4f %9.4f\n',n1(1)+yp1(1),n1(2)+yp1(2),n1(3)+yp1(3));
% Applying point force at Commissure 1 in direction R1
% LCID 1, CID 1
fprintf(fid, '*LOAD_NODE_POINT\n');
fprintf(fid, '$      NID       DOF      LCID        SF       CID\n');
fprintf(fid, '%10i %9i %9i %9.4f %9i\n',par.NodeLandmarkUvent,1,1,force1,1);

%--------- Commissure 2 -----------%
% Resultant unit vector at Commissure 2
R2 = (n2-n1)/norm(n2-n1) + (n2-n3)/norm(n2-n3);
R2 = R2/norm(R2);
% calculating unit vector x' in global coordinate system
xp2 = R2;
% calculating unit vector y' in global coordinate system
yp2 = -cross(xp2,zu);
yp2 = yp2/norm(yp2);
% CID 2
fprintf(fid, '*DEFINE_COORDINATE_SYSTEM\n');
fprintf(fid, '$      CID        XO        YO        ZO        XL        YL        ZL      CIDL\n');
fprintf(fid, '%10i %9.4f %9.4f %9.4f %9.4f %9.4f %9.4f %9i\n',2,n2(1),n2(2),n2(3),n2(1)+xp2(1),n2(2)+xp2(2),n2(3)+xp2
fprintf(fid, '$       XP        YP        ZP\n');
fprintf(fid, '%10.4f %9.4f %9.4f\n',n2(1)+yp2(1),n2(2)+yp2(2),n2(3)+yp2(3));
% Applying point force2 at Commissure 2 in direction R2
% LCID 1, CID 2
fprintf(fid, '*LOAD_NODE_POINT\n');
fprintf(fid, '$      NID       DOF      LCID        SF       CID\n');
fprintf(fid, '%10i %9i %9i %9.4f %9i\n',par.NodeLandmarkVvent,1,1,force2,2);

%--------- Commissure 3 -----------%
% Resultant unit vector at Commissure 3
R3 = (n3-n2)/norm(n3-n2) + (n3-n1)/norm(n3-n1);
R3 = R3/norm(R3);
% calculating unit vector x' in global coordinate system
xp3 = R3;
```

```
% calculating unit vector y' in global coordinate system
yp3 = -cross(xp3,zu);
yp3 = yp3/norm(yp3);
% CID 3
fprintf(fid, '*DEFINE_COORDINATE_SYSTEM\n');
fprintf(fid, '$      CID        XO        YO        ZO        XL        YL        ZL      CIDL\n');
fprintf(fid, '%10i %9.4f %9.4f %9.4f %9.4f %9.4f %9.4f %9i\n',3,n3(1),n3(2),n3(3),n3(1)+xp3(1),n3(2)+xp3(2),n3(3)+xp3
fprintf(fid, '$       XP        YP        ZP\n');
fprintf(fid, '%10.4f %9.4f %9.4f\n',n3(1)+yp3(1),n3(2)+yp3(2),n3(3)+yp3(3));
% Applying point force3 at Commissure 3 in direction R3
% LCID 1, CID 3
fprintf(fid, '*LOAD_NODE_POINT\n');
fprintf(fid, '$      NID       DOF      LCID        SF       CID\n');
fprintf(fid, '%10i %9i %9i %9.4f %9i\n',par.NodeLandmarkWvent,1,1,force3,3);

% ***** MIDDLES OF FREE MARGINS
% Inward-downward radial forces to be applied
forceM1 = 0.13; % Newtons
forceM2 = 0.13; % Newtons
forceM3 = 0.13; % Newtons

m1 = [xn(1,par.NodesLH1aort(end));...
      yn(1,par.NodesLH1aort(end));...
      zn(1,par.NodesLH1aort(end))]; % coordinates of Middle 1
m2 = [xn(1,par.NodesLH2aort(end));...
      yn(1,par.NodesLH2aort(end));...
      zn(1,par.NodesLH2aort(end))]; % coordinates of Middle 2
m3 = [xn(1,par.NodesLH3aort(end));...
      yn(1,par.NodesLH3aort(end));...
      zn(1,par.NodesLH3aort(end))]; % coordinates of Middle 3

%{
% Coordinates of centre of leaflet attchement lines nadirs
[mb,~] = Circle3pts(scaledLandmarks.D,...
        scaledLandmarks.E,scaledLandmarks.F);
%}
% Coordinates of centre of m1, m2, m3
[mb,~] = Circle3pts(m1,m2,m3);

%--------- Middle 1 -----------%
% calculating unit vector x' in global coordinate system
xp1 = (mb-m1)/norm(mb-m1);
% calculating unit vector y' in global coordinate system
yp1 = -cross(xp1,zu);
yp1 = yp1/norm(yp1);
% CID 4
fprintf(fid, '*DEFINE_COORDINATE_SYSTEM\n');
fprintf(fid, '$      CID        XO        YO        ZO        XL        YL        ZL      CIDL\n');
fprintf(fid, '%10i %9.4f %9.4f %9.4f %9.4f %9.4f %9.4f %9i\n',4,m1(1),m1(2),m1(3),m1(1)+xp1(1),m1(2)+xp1(2),m1(3)+xp1
fprintf(fid, '$       XP        YP        ZP\n');
fprintf(fid, '%10.4f %9.4f %9.4f\n',m1(1)+yp1(1),m1(2)+yp1(2),m1(3)+yp1(3));
```

```
% Applying point force at Middle 1 in direction xp1
% LCID 1, CID 4
fprintf(fid, '*LOAD_NODE_POINT\n');
fprintf(fid, '$      NID       DOF      LCID        SF       CID\n');
fprintf(fid, '%10i %9i %9i %9.4f %9i\n',par.NodesLH1aort(end),1,1,forceM1/2,4);
fprintf(fid, '%10i %9i %9i %9.4f %9i\n',par.NodesLH1aort(end-1),1,1,forceM1/2,4);


%--------- Middle 2 -----------%
% calculating unit vector x' in global coordinate system
xp2 = (mb-m2)/norm(mb-m2);
% calculating unit vector y' in global coordinate system
yp2 = -cross(xp2,zu);
yp2 = yp2/norm(yp2);
% CID 5
fprintf(fid, '*DEFINE_COORDINATE_SYSTEM\n');
fprintf(fid, '$      CID        XO        YO        ZO        XL        YL        ZL      CIDL\n');
fprintf(fid, '%10i %9.4f %9.4f %9.4f %9.4f %9.4f %9.4f %9i\n',5,m2(1),m2(2),m2(3),m2(1)+xp2(1),m2(2)+xp2(2),m2(3)+xp2
fprintf(fid, '$       XP        YP        ZP\n');
fprintf(fid, '%10.4f %9.4f %9.4f\n',m2(1)+yp2(1),m2(2)+yp2(2),m2(3)+yp2(3));
% Applying point force at Middle 2 in direction xp2
% LCID 1, CID 5
fprintf(fid, '*LOAD_NODE_POINT\n');
fprintf(fid, '$      NID       DOF      LCID        SF       CID\n');
fprintf(fid, '%10i %9i %9i %9.4f %9i\n',par.NodesLH2aort(end),1,1,forceM2/2,5);
fprintf(fid, '%10i %9i %9i %9.4f %9i\n',par.NodesLH2aort(end-1),1,1,forceM2/2,5);
```

```
%--------- Middle 3 -----------%
% calculating unit vector x' in global coordinate system
xp3 = (mb-m3)/norm(mb-m3);
% calculating unit vector y' in global coordinate system
yp3 = -cross(xp3,zu);
yp3 = yp3/norm(yp3);
% CID 6
fprintf(fid, '*DEFINE_COORDINATE_SYSTEM\n');
fprintf(fid, '$      CID        XO        YO        ZO        XL        YL        ZL      CIDL\n');
fprintf(fid, '%10i %9.4f %9.4f %9.4f %9.4f %9.4f %9.4f %9i\n',6,m3(1),m3(2),m3(3),m3(1)+xp3(1),m3(2)+xp3(2),m3(3)+xp3
fprintf(fid, '$       XP        YP        ZP\n');
fprintf(fid, '%10.4f %9.4f %9.4f\n',m3(1)+yp3(1),m3(2)+yp3(2),m3(3)+yp3(3));
% Applying point force at Middle 3 in direction xp3
% LCID 1, CID 6
fprintf(fid, '*LOAD_NODE_POINT\n');
fprintf(fid, '$      NID       DOF      LCID        SF       CID\n');
fprintf(fid, '%10i %9i %9i %9.4f %9i\n',par.NodesLH3aort(end),1,1,forceM3/2,6);
fprintf(fid, '%10i %9i %9i %9.4f %9i\n',par.NodesLH3aort(end-1),1,1,forceM3/2,6);
```